Gastroenterology 2021;161:1288–1302

Recurrent Frameshift Neoantigen Vaccine Elicits Protective Immunity With Reduced Tumor Burden and Improved Overall Survival in a Lynch Syndrome Mouse Model

Johannes Gebert,[1,2] Ozkan Gelincik,[3] Mine Oezcan-Wahlbrink,[1,2] Jason D. Marshall,[4] Alejandro Hernandez-Sanchez,[1,2] Katharina Urban,[1,2] Mark Long,[5] Eduardo Cortes,[5] Elena Tosti,[6] Eva-Maria Katzenmaier,[1,2] Yurong Song,[4] Ali Elsaadi,[3] Nan Deng,[7] Eduardo Vilar,[7] Vera Fuchs,[1,2] Nina Nelius,[1,2] Yan P. Yuan,[8] Aysel Ahadova,[1,2] Shizuko Sei,[9] Robert H. Shoemaker,[9] Asad Umar,[9] Lei Wei,[5] Song Liu,[5] Peer Bork,[8,10,11] Winfried Edelmann,[6] Magnus von Knebel Doeberitz,[1,2] Steven M. Lipkin,[3] and Matthias Kloor[1,2]

[1]Department of Applied Tumor Biology, Institute of Pathology, University of Heidelberg, Heidelberg, Germany; [2]Clinical Cooperation Unit Applied Tumor Biology, German Cancer Research Center, Heidelberg, Germany; [3]Weill Cornell Medical College, New York, New York; [4]Cancer ImmunoPrevention Laboratory, Frederick National Laboratory for Cancer Research, Frederick, Maryland; [5]Department of Biostatistics and Bioinformatics, Roswell Park Comprehensive Cancer Center, Buffalo, New York; [6]Department of Cell Biology, Albert Einstein College of Medicine, New York, New York; [7]Department of Clinical Cancer Prevention, The University of Texas MD Anderson Cancer Center, Houston, Texas; [8]European Molecular Biology Laboratory, Structural and Computational Biology Unit, Heidelberg, Germany; [9]Division of Cancer Prevention, National Cancer Institute, Bethesda, Maryland; [10]Max Delbrück Centre for Molecular Medicine, Berlin, Germany; and [11]Department of Bioinformatics, Biocenter, University of Würzburg, Würzburg, Germany

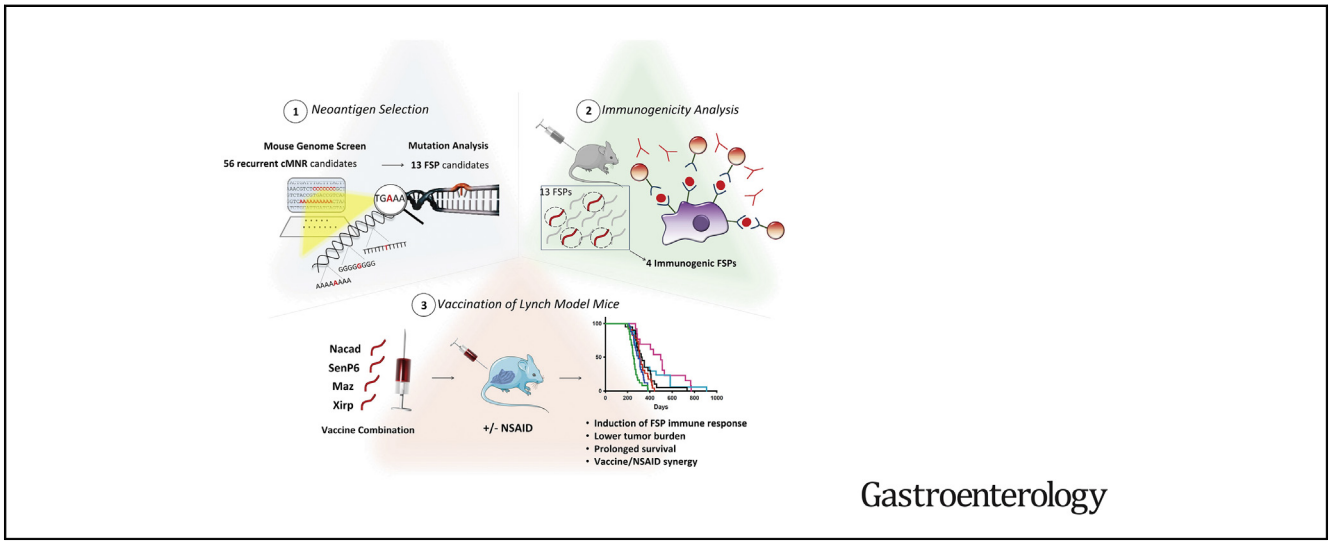

BACKGROUND & AIMS: DNA mismatch repair deficiency drives microsatellite instability (MSI). Cells with MSI accumulate numerous frameshift mutations. Frameshift mutations affecting cancer-related genes may promote tumorigenesis and, therefore, are shared among independently arising MSI tumors. Consequently, such recurrent frameshift mutations can give rise to shared immunogenic frameshift peptides (FSPs) that represent ideal candidates for a vaccine against MSI cancer. Pathogenic germline variants of mismatch repair genes cause Lynch syndrome (LS), a hereditary cancer syndrome affecting approximately 20–25 million individuals worldwide. Individuals with LS are at high risk of developing MSI cancer. Previously, we demonstrated safety and immunogenicity of an FSP-based vaccine in a phase I/IIa clinical trial in patients with a history of MSI colorectal cancer. However, the cancer-preventive effect of FSP vaccination in the scenario of LS has not yet been demonstrated. **METHODS:** A genome-wide database of 488,235 mouse coding mononucleotide repeats was established, from which a set of candidates was selected based on repeat length, gene expression, and mutation frequency. In silico prediction, in vivo immunogenicity testing, and epitope mapping was used to identify candidates for FSP vaccination. **RESULTS:** We identified 4 shared FSP neoantigens (Nacad [FSP-1], Maz [FSP-1], Senp6 [FSP-1], Xirp1 [FSP-1]) that induced CD4/CD8 T cell responses in naïve *C57BL/6* mice. Using *VCMsh2* mice, which have a conditional knockout of Msh2 in the intestinal tract and develop intestinal cancer, we showed vaccination with a combination of only 4 FSPs significantly

increased FSP-specific adaptive immunity, reduced intestinal tumor burden, and prolonged overall survival. Combination of FSP vaccination with daily naproxen treatment potentiated immune response, delayed tumor growth, and prolonged survival even more effectively than FSP vaccination alone. **CONCLUSIONS:** Our preclinical findings support a clinical strategy of recurrent FSP neoantigen vaccination for LS cancer immunoprevention.

Keywords: Colorectal Cancer; Frameshift Neoantigens; Lynch Syndrome; Mouse Model; Preventive Cancer Vaccine.

WHAT YOU NEED TO KNOW

BACKGROUND AND CONTEXT

Lynch syndrome tumors are characterized by DNA mismatch repair deficiency and microsatellite instability, which gives rise to tumor-specific, mutation-induced, frameshift peptide neoantigens.

NEW FINDINGS

We demonstrate, in a hereditary cancer model, that tumor prevention by vaccination with mutation-induced neoantigens is feasible and effective.

LIMITATIONS

The results are restricted to a mouse model, and clinical effectiveness of a tumor-preventive neoantigen-based vaccine needs to be demonstrated in a clinical trial.

IMPACT

Vaccination against microsatellite instability–induced frameshift peptide neoantigens prevents tumors in a mouse model. The vaccine strategy therefore holds great promise for individuals with Lynch syndrome.

Mismatch repair deficiency (MMRD) is an important mechanism driving mutagenesis and genomic instability in human cancers. MMR-deficient cells accumulate numerous somatic mutations, including insertion/deletion (indel) mutations, predominantly altering repetitive microsatellite (MS) sequences.[1,2] Indels in coding MS promote translational frameshifts, which also generate truncated frameshift peptide (FSP)-encoding neoproteins.[3] Several studies have identified a large spectrum of genes affected by such frameshift mutations, demonstrating that indel mutations affecting key tumor suppressors, such as the *TGFBR2*, are enriched in MMRD cancers.[4–6]

MMRD cancers can develop sporadically or from hereditary predisposition as part of Lynch syndrome (LS). LS causes up to 2%–5% of all colorectal cancers (CRCs),[7] as well as endometrial, ovarian, uroepithelial, and other cancers.[8] The estimated population incidence of LS is 1:225–1:360.[9,10] Affected individuals have an estimated 20%–70% lifetime risk of developing cancer.[11,12] LS is caused mainly by heterozygous germline mutations in one of the MMR genes *MSH2*, *MLH1*, *MSH6*, or *PMS2*.[13,14] Inactivation of both alleles of an individual MMR gene is required to cause the MMRD, typically by somatic "second hit" inactivation of the functional MMR allele.[15,16]

MMRD CRCs display distinct clinicohistopathologic features that are directly related to the high FSP load. Most importantly, these include increased infiltration with lymphocytes, memory T cells, and improved survival compared to patients with low tumor-infiltrating lymphocyte CRC.[17–19] Accordingly, MMRD tumors are among the most responsive to immune checkpoint inhibitors that enhance endogenous anti-tumor adaptive immunity, which is driven predominantly by FSPs.[20]

The existence of shared FSP neoantigens in MMRD cancers creates a mechanism-based framework for novel tumor immunopreventive approaches.[3] Immunologic studies performed by our group and others have identified several immunogenic microsatellite instability (MSI)-associated FSPs in MMRD CRCs that are recognized by, and promote proliferation of, cytotoxic T cells.[21,22] Importantly, endogenous adaptive immunity against FSPs is detected in MMRD cancer patients, and also in tumor-free LS "previvors," suggesting a role for immune surveillance in LS mutation carriers.[23]

Vaccination with recurrent FSPs that are shared by multiple MMRD tumors of different patients is a promising approach to boost immune surveillance of MMRD precancerous cell clones, and potentially immune-interception of subclinical MMRD tumors for effective immunoprevention.[3] Recently, we performed a therapeutic phase IIa clinical trial demonstrating the safety and immunologic efficacy of a trivalent recurrent FSP-based vaccine in patients with a history of MMRD MSI CRC.[24] However, whether recurrent FSP vaccination can reduce LS/sporadic MMRD tumor burden and prolong patient survival, in addition to boosting anti-tumor immunity, is unknown.

Nonsteroidal anti-inflammatory drugs (NSAIDs), particularly aspirin (acetylsalicylic acid [ASA]), have been studied intensively for gastrointestinal cancer prevention. NSAIDs reduce cyclooxygenase-1 and -2 production of prostaglandin E2, which binds to EP1–4 receptors.[25] Prostaglandin E2 drives intestinal tumorigenesis by both promoting protumorigenic EP2/4-driven intestinal epithelial and stem cell proliferation and inhibiting immune surveillance and immune-interception of tumor neoantigens.[26,27] ASA reduces LS CRC incidence and is widely used for LS gastrointestinal cancer prevention.[25,28] However, a recent large-scale (approximately 20,000 participants) randomized clinical trial in community-dwelling older (65 years and older) men and women has raised questions about whether

Abbreviations used in this paper: **ASA, acetylsalicylic acid; cMNR, coding mononucleotide repeat; CRC, colorectal cancer; FSP, frameshift peptide; IFN, interferon; LS, Lynch syndrome; MMRD, mismatch repair deficiency; MS, microsatellite; MSI, microsatellite instability; NAP, naproxen; NSAID, nonsteroidal anti-inflammatory drug; OVA, ovalbumin.**

Most current article

0016-5085
https://doi.org/10.1053/j.gastro.2021.06.073

ASA might actually increase overall pan-cancer rates and mortality, at least in older adults.[29] Recently, naproxen (NAP), a propionic acid NSAID derivative, has shown pronounced cancer-preventive activity in LS mouse models and increased immune surveillance in LS patients.[30,31]

LS mouse models have provided many important mechanistic and translational insights. Intestinal epithelial-specific MMRD mouse models, such as *VCMsh2*,[32] closely resemble the clinical phenotype seen in LS CRC patients because they specifically develop intestinal tumors, whereas constitutional MMRD mice (eg, *Msh2*^{null}) most frequently develop T cell lymphomas, which confounds survival analysis.[33] Previously, we described a set of candidate coding mononucleotide repeat (cMNR) frameshift mutations in a small number of MSI mouse tumors and detected human/mouse orthologous conserved cMNR repeats.[34] Here, we used *VCMsh2* mice to test the hypothesis that recurrent FSP vaccination alone or in combination with NSAID treatment can promote anti-FSP adaptive immunity sufficiently to reduce intestinal tumor burden and prolong overall survival.

Materials and Methods

Selection of Frameshift Peptides for Vaccination

Computational analysis of mouse genome to identify coding microsatellites. Search tools and algorithms developed and applied previously for the human cMNR database (www.seltarbase.de)[34–36] were adapted accordingly to detect all cMNRs in the mouse genome. Perl scripts were developed to use the ensembl API (www.ensembl.org/info/docs/api/) and a rigorous redundancy check at the 98% level was applied. All annotation-based cMNRs with a minimal repeat length of 4 mononucleotides were retrieved. Using several filters, repeat tracts within pseudogenes, vector sequences, as well as homopolymeric nucleotide stretches at the most 5′ or 3′ ends of sequences, were excluded. Candidate sequences were stored in a relational database for further analysis (http://www.bork.embl.de/Docu/yuan/rpt/). Processing through this analysis pipeline was based on gene sequence data of the *Mus musculus* Ensembl release version 77_38.

Mutation and expression analysis of coding mononucleotide repeats in *VCMsh2* formalin-fixed, paraffin-embedded tumors. For MSI classification of identified tumors, 4 long noncoding MS markers were used (mA24, mA27, mT27, and mA33z[34,37]). Marker MSI was defined by the occurrence of novel peaks in tumor compared to normal tissue. Tumor was scored as MSI if at least 1 of 4 markers showed instability. For polymerase chain reaction–based indel mutation analysis, a candidate set of 56 cMNRs (Supplementary Figure 1 and Supplementary Table 1) was selected. These cMNR candidates were chosen based on repeat length (8 or more nucleotides), representation of all 4 nucleotides, transcript isoform coverage, and robust cMNR amplification.

Predicted Computational NetMHC and SYFPETHI Immunogenicity of frameshift peptides. To predict the potential immunogenicity of FSPs resulting from cMNR mutations, peptide sequences were submitted to online available epitope prediction tools SYFPEITHI (www.syfpeithi.de) and netMHC4.0 (http://www.cbs.dtu.dk/services/NetMHC/). Searches were performed for major histocompatibility complex (MHC) class I antigens present in *C57BL/6* mice (H2-*Db* and -*Kb* alleles). For SYFPEITHI, the calculated score was recorded, for netMHC4.0, the predicted percentage rank indicating MHC binding likelihood and the number of predicted strong binders and weak binders (corresponding to an affinity lower than 50 μM and 500 μM, respectively) were recorded for each peptide.

Evaluation of frameshift peptide immunogenicity in *C57BL/6* mice. FSPs were synthesized by Genaxxon (Ulm, Germany). Details of peptide solution are described in the Supplementary Material. For preparation of the vaccine formulations, 50 μg of 3 to 4 FSPs were mixed with 50 μg of ovalbumin (OVA) 257–264 and OVA 323–339 each and 20 μg CpG ODN 1826; the mixture was suspended in a final injection volume of 50 μL in phosphate-buffered saline.

Control vaccine formulations without FSPs was prepared as described above, adding phosphate-buffered saline in place of the FSPs. Vaccine mixes were administered 4 times in biweekly intervals to *C57BL/6* mice. All vaccines were administered subcutaneously into the left or right flank of each mouse. One week after the last vaccination, cellular immune responses were measured using interferon (IFN)-gamma enzyme-linked immunosorbent spot (ELISpot) assay from splenocytes. Humoral FSP-specific immune responses were measured using peptide enzyme-linked immunosorbent assay. Reactions significantly above background after subtraction of no-peptide control spots and SDs of the peptide and the control spot counts were considered as positive. Assays for determining cellular and humoral immune responses were performed according to previously established protocols described in the Supplementary Material. Detailed protocols for adjuvant optimization are provided in the Supplementary Material.

Immunoprevention in VCMsh2 *Mice*

Mouse strains and tissue collection. Villin-Cre mice were bred to *Msh2* $^{LoxP/LoxP}$ mice to generate *VCMsh2* mice in the laboratory of Winfried Edelmann previously.[32] Mice were genotyped to confirm the status of *Cre* transgene and floxed *Msh2*, respectively. Mice with the *Villin* promoter used to drive expression of Cre recombinase and *Msh2* exon 12 flanked by *LoxP* sites (*VCMsh2*) mice on the *C57BL/6* genetic background[32] were bred and housed in a specific pathogen–free barrier facility at Weill Cornell Medical College according to Institutional Animal Care and Use Committee guidelines.

Cancer prevention and vaccination protocols. Control mice were given pelleted plain New Western Diet 1 (Research Diets). ASA and NAP were purchased from Spectrum Chemicals Inc in powder form. ASA- or NAP-impregnated, pelleted New Western Diet 1 (400 ppm ASA or 166 ppm NAP) were given at the age of weaning to mice assigned to those arms. For FSP vaccination, all peptides (Nacad [FSP-1], Xirp1 [FSP-1], Maz [FSP-1]), and Senp6 [FSP-1]) were custom made by Thermo Fisher Scientific at >98% purity and the adjuvant CpG ODN1826 was purchased from InvivoGen. Vaccine components were prepared following manufacturer's protocol in dimethyl sulfoxide and combined fresh before each vaccination. The study consists of the following 6 arms: controls, vaccine only, NAP only, ASA only, vaccine + NAP, and vaccine + ASA. Starting at the age of 6–8 weeks, mice enrolled in FSP vaccine alone and FSP vaccine + NSAID arms were

vaccinated subcutaneously in either left or right hind 4 times biweekly, followed by 4 times monthly. Per shot, each mouse received 50 μg of each FSP combined with 20 μg of the adjuvant.

Each treatment group was populated with 16–20 mice on a rolling basis for efficacy studies. Mice were monitored over their lifetime by Research Animal Resources and Compliance Veterinary Services and the investigator twice a week for the following signs to determine euthanasia: weight loss, poor coat quality, hunched posture, and pale limbs (anemia). Following the Institutional Animal Care and Use Committee guidelines, mice presenting with these signs were euthanized by CO_2 inhalation.

Regulatory compliance. All *VCMsh2* mice were housed in isolation units approved by the Weill Cornell Institutional Animal Care and Use Committee (protocol number: AC-AAAN5700). The mice used in trials were allowed to run free in the cage, were fed the Western diet or NSAID-containing matched diet (Research Diets), and were provided water ad libitum. The Animal Care Facilities at German Cancer Research Center were used for housing *C57BL/6* mice for frameshift peptide selection. The German Cancer Research Center facilities have been approved by The Federation of European Laboratory Animal Science Associations and accredited. Adjuvant optimization studies were performed in the Frederic National laboratory according to Institutional Review Board and Animal Care and Use Committee regulations.

Immunohistochemistry. Immunohistochemistry staining was performed on formalin-fixed, paraffin-embedded tissues from intestinal tumors taken from *VCMsh2* mice treated with NAP with or without the tetravalent FSPs vaccine according to standard protocols (see Supplementary Methods). The following primary antibodies were used for CD3: clone SP7 abcam ab16669; for CD4: clone 4SM95 ThermoFisher Scientific #14-9766-82; for CD8: clone 4SM15 ThermoFisher Scientific #14-0808-82; for Foxp3: clone FJK-16s ThermoFisher Scientific #14-5773-82; for PD-1: clone EPR20665 abcam ab214421. The following biotinylated secondary antibodies were used for CD3 and PD-1: Vector Laboratories BA-1100; and for CD4, CD8 and Foxp3: Vector Laboratories BA-9401.

Immune cell quantification. The tissue slides were scanned with a NanoZoomer S210 slide scanner (Hamamatsu, Japan) with a scanning resolution of 0.23 μm/pixel in the 40$\times$ mode. The 3,3′-diaminobenzidine tetra hydrochloride chromogen–positive stained cells were identified with QuPath (version 0.1.2[38]) using the positive cell detection feature in at least 1 region of interest with an area of 0.25 mm^2 within each tumor slide. The number of positive cells was counted and recorded. Tissue sections with insufficient quality or with no staining signal detectable in the entire section were excluded from the analysis.

Statistical evaluation. Mann-Whitney tests comparing the FSP vaccine group with the control group were performed using GraphPad Prism software, version 8.2.1 for Windows (GraphPad Software, San Diego, CA). GraphPad was also used to generate dot plots. Mann-Whitney comparisons of tumor burden (sum of all intestinal tumor weights per mouse) and Kaplan-Meier curve overall survival analyses were also performed using GraphPad Prism. Statistical analyses of adjuvant comparison results were conducted with GraphPad Prism 7 software using one-way analysis of variance nonparametric analysis with the Kruskal-Wallis multiple comparisons test. $P < .05$ was considered significant.

Results

Computational Identification of Mouse Genome Coding Microsatellites

A multistep strategy was employed to develop a mouse vaccine composed of the most immunogenic FSP candidates and to test their efficacy in immunocompetent *VCMsh2* mice (Figure 1).

Using a computational approach, we established a genome-wide database of coding MS in the mouse genome. This database comprises 488,235 cMNRs consisting of 4 or more nucleotides in length (Figure 2). Because increased repeat length correlates with increased cMNR mutation probability,[5,6] we focused our subsequent analyses on cMNRs with a repeat length of 8 or more nucleotides.

Coding Mononucleotide Repeat Frameshift Mutation Patterns in Intestinal Tumors of VCMsh2 *Mice*

For mutational analyses of candidate cMNRs, intestinal adenomas and carcinomas, as well as normal mucosae, from the same animals were collected from *VCMsh2* mice (n = 25; aged between 7 and 15 months, 1 tumor per animal). Tumors were confirmed as MSI/MMRD when analyzed by a panel of mononucleotide repeats (mA24, mA27, mT27, and mA33) previously established as sensitive and specific for MSI detection in mouse tumors.[5] Frameshift mutation analyses were performed on a selected subset of 56 cMNR candidates that showed increased repeat length (8 or more nucleotides), represented all 4 nucleobases, covered different transcript isoforms, and allowed robust amplification from formalin-fixed, paraffin-embedded tissue specimens (Supplementary Figure 1). The majority of these cMNR candidates (36 of 56 [64.3%]) carried frameshift mutations in 1 or more tumors, with mutation frequencies ranging from 6.5% to 75% (Supplementary Figure 1). After eliminating candidates polymorphic in normal tissue and/or showing a mutation frequency of <15% in tumors, we further evaluated 13 remaining cMNR candidate genes and confirmed their expression in normal and tumor tissues by reverse transcription polymerase chain reaction.

In Silico Prediction of Frameshift Peptide Immunogenicity

We next searched for potential immunogenic MHC binding motifs in 26 FSP neopeptides derived from (−1) and (−2) indel mutations affecting these 13 cMNRs (Table 1). Using epitope prediction tools netMHC4.0 and SYFPEITHI 1.0, a subset of 10 FSPs turned up as potentially immunogenic candidates and were selected for subsequent

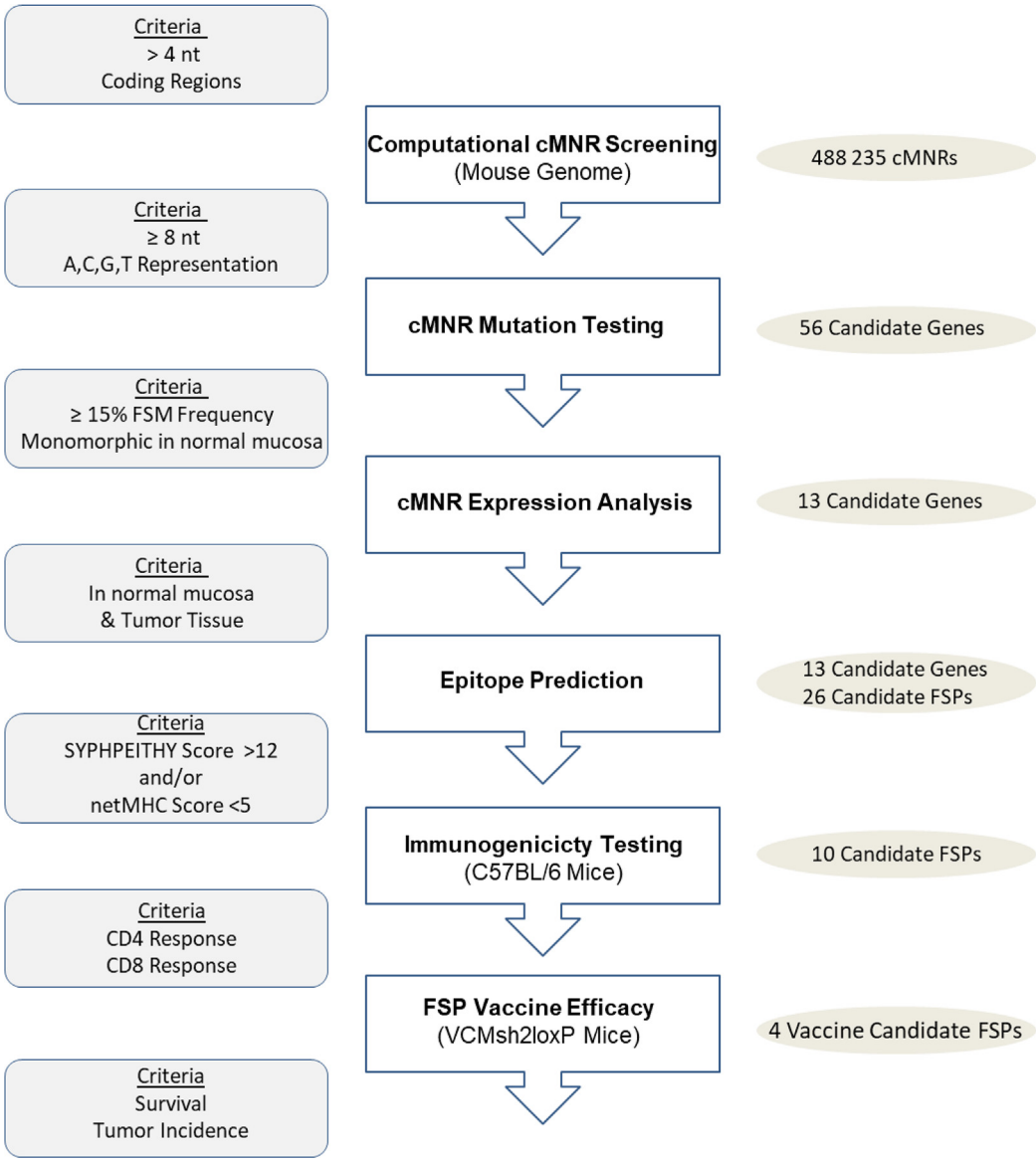

Figure 1. Experimental strategy for developing a murine FSP vaccine.

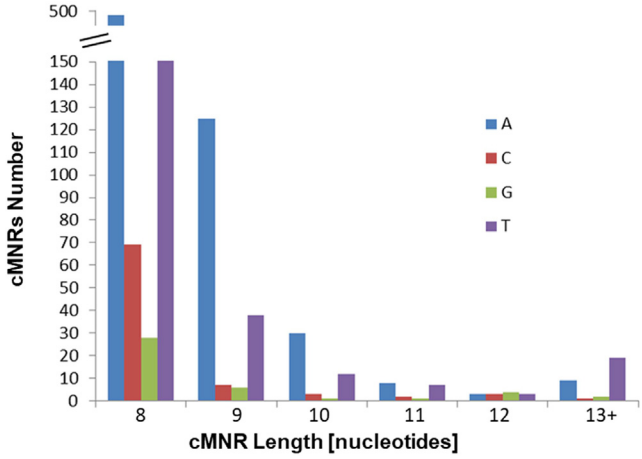

Figure 2. Distribution of cMNRs in the mouse genome. The occurrence of cMNRs is shown according to repeat type and length (8 or more nucleotides).

immunologic analyses. Based on our mutation data, these 10 FSPs covered most of the analyzed tumors (15 of 16 [93%])

Induction of Frameshift Peptide–Specific Cellular and Humoral Immune Responses in C57BL/6 *Mice*

The immunogenicity of 10 FSPs with highest in silico prediction scores was experimentally evaluated in *C57BL/6* mice (Figure 3*A*). To determine induction of antigen-specific T cell responses, ex vivo IFN-gamma ELISpot assays were performed. Four of 10 FSP neoantigens, that is, Maz (FSP-1), Nacad (FSP-1), Xirp1 (FSP-1), and Senp6 (FSP-1), triggered the induction of T cell responses significantly above background in vaccinated *C57BL/6* mice (Figure 3*B*). Vaccination was repeated using a mixture of the 4 positive candidates, and ELISpot was repeated for each peptide separately to validate the immunogenicity of FSP neoantigens when

Table 1. Mutation frequency of cMNR and FSP Sequences

Gene	cMNR		Intestinal expression		Mutation frequency, %			WT FSP sequence	SYFPEITHI score	netMHC		
	Type	Monomorphic	Normal	Tumor	Total	FS-specific				Db	Kb	% Rank
Nacad	C14	Yes	Yes	Yes	75	FS(–1)	56.25	VIYAPPPP**AEGRWPCWLLRAH***[a]	15	s0 w0	s0 w0	3
						FS(–2)	37.5	DVIYAPPP**QQRGGGRAGYSERIDGQRDRETGVSAGTR PGHARGGCGR***[a]	14	s0 w0	s0 w0	6
Xirp1	C9	Yes	Yes	Yes	37.5	FS(–1)	31.25	GKGPGGPP**LSSPKRVMYRLSVGCLRPTL***[a]	19	s0 w2	s1 w4	0.4
						FS(–2)	6.25	GKGPGGPP*	—	—	—	—
5730596B20Rik	C12	Yes	Yes	Yes	37.5	FS(–1)	37.5	GTLPPPPP**TQH***	6	s0 w0	s0 w0	39
						FS(–2)	0.00	LGTLPPPP**QPSTEQSGWKHHQ***	7	s0 w0	s0 w0	55
Rif1	A12	Yes	Yes	Yes	33.3	FS(–1)	20.00	AHTDKKKK*	—	—	—	—
						FS(–2)	13.33	AHTKDKKK**SETVGQTETRIFISKNKEW***[a]	15	s0 w0	s0 w0	4.5
Maz	C8	Yes	Yes	Yes	33.3	FS(–1)	20.00	PCTLLAPP**SPCWAWTPGGWAAS***	7	s0 w0	s0 w0	9.5
						FS(–2)	13.33	FPCTLLAP**LPRAGPGLPGGGRPHELLPATSGSRP EPPAGRG***[a]	17	s0 w0	s0 w0	3.5
Hic1	C10	Yes	Yes	Yes	31.25	FS(–1)	18.75	DRTFPSPP**RIGAI***[a]	14	s0 w0	s0 w0	5
						FS(–2)	12.5	DRTFPSPP**ELARYNI***	18	s0 w0	s0 w0	4.5
Sdccag1	A11	Yes	Yes	Yes	25	FS(–1)	25.00	EAPKGKKK**SKRTSSCRSRRRTSRCL***[a]	12	s0 w0	s0 w0	8
						FS(–2)	6.25	EAPKGKKK**AKEQAAAEAAEEQAAACRCGSQPV SLCQCQKIL***	16	s0 w0	s0 w0	2.5
Tmem107	G9	Yes	Yes	Yes	25	FS(–1)	25.00	TQYFGMGG**VVENRSQI***[a]	24	s2 w1	s0 w0	0.5
						FS(–2)	6.25	TQYFGMGG**WWKIDPKSEGFPHLDLSCTCEIGRVLKS HTHPNPPAYKVWRFKCLGWKGL***	21	s0 w0	s1 w2	0.25
Srcin1	C9	Yes	Yes	Yes	25	FS(–1)	25.00	DEGMWPPP**TTS***	6	s0 w0	s0 w0	31
						FS(–2)	0.00	VDEGMWPP**QQPPEPVPQEGGS***	12	s0 w0	s0 w0	22
Marcks	A11	Yes	Yes	Yes	20	FS(–1)	20.00	SSETPKKK**RSAFPSRSPSS***[a]	12	s0 w0	s0 w0	5.5
						FS(–2)	0.00	SSETPKKK**EALFLQEVLQAERLLLQEEQEGVGRGR***	16	s0 w3	s0 w0	0.8
Senp6	A11	Yes	Yes	Yes	18.75	FS(–1)	18.75	VKCSMKKK**IMLSMKMKNQVTENLRARTFVIEPK VRMASGMNASVLYIIQMP***[a]	27	s10 w12	s0 w2	0.03
						FS(–2)	0.00	VKCSMKKK**SCYQ***	1	s0 w0	s0 w0	20

Table 1. Continued

Gene	cMNR		Intestinal expression		Mutation frequency, %		WT FSP sequence	SYFPEITHI	netMHC		
	Type	Monomorphic	Normal	Tumor	Total	FS-specific		score	Db	Kb	% Rank
Phactr4	A10	Yes	Yes	Yes	18.75	FS(–1) 18.75	PWKWRKKKK**AVISSKRHQKF***	12	s0 w0	s0 w0	3.5
						FS(–2) 0.00	PWKWRKKK**Q***	2	s0 w0	s0 w0	75
Chmb2	C10	Yes	Yes	Yes	18.75	FS(–1) 12.5	VRTRPSPP**HLSPASWVLKPFAINAKGIFLILCGNWQQGCL CHLGMHLRHRQVGL***	21	s1 w3	s0 w1	0.5
						FS(–2) 6.25	VRTRPSPP**ISLQPHGS***	16	s0 w0	s0 w0	11

NOTE. Genes affected by cMNR FS mutations and derived FSPs. Predicted immunoscores for FSPs (in boldy type) including an 8 amino acid wild-type (WT) sequence are indicated for *C57BL/6* alleles H2-Db and H2-Kb (SYFPEITHI 1.0 and netMHC4.0). The numbers of strong (s) and weak (w) binders are shown. Low numbers of percent rank (% rank), as well as SYFPEITHI scores >12, predict strong MHC binding.
[a]FSPs used for further analysis.

administered mixed together. Separate analysis of CD4 and CD8 T cell responses demonstrated that Maz (FSP-1) and Senp6 (FSP-1) elicited CD4 T cell responses, whereas Xirp1 (FSP-1) predominantly induced a CD8 T cell response. Nacad (FSP-1) induced both CD4 and CD8 T cell responses (Figure 3*C*). Characterization of the immunogenic regions of the FSPs by using shorter peptide fragments from the N- and C-terminal part of the FSPs demonstrated that the immunogenic parts of Xirp1 (FSP-1) and Senp6 (FSP-1) are located at the C-terminus of their FSPs in contrast to Nacad (FSP-1), the immunogenic region of which resides within the N-terminus of this FSP. A mixed pattern was observed for Maz (FSP-1), which is immunogenic as a whole in both parts of the FSP. Epitope location was correlated with in silico predictions (Figure 3*D*). Potential immunogenicity of wild-type peptide stretches at the N-terminus was excluded because cross-reactivity with the respective wild-type protein sequences was observed (Supplementary Figure 2). Three FSPs—Nacad (FSP-1), Senp6 (FSP-1), and Maz (FSP-1)—also elicited a humoral immune responses detectable by peptide enzyme-linked immunosorbent assay (Supplementary Figure 3).

Early Occurrence of Recurrent Frameshift Peptide Mutations in VCMsh2 *Intestinal Tumors*

We evaluated a separate nonoverlapping cohort of 7-month-old *VCMsh2* mice (n = 16 mice, 25 tumors) fed a regular chow diet to test whether recurrent *Maz*, *Nacad*, *Senp6*, and *Xirp1* FSPs are early mutations that could serve as candidate vaccine neoantigens. *VCMsh2* mice develop intestinal tumors starting at age 6–9 months.[32] When MSI tumors (n = 16) were tested for FS mutations, moderate to high frequencies were observed for *Nacad* (–1) (50%), *Senp6* (–1) (25%), and *Maz* (–1) (6%). Thus, even tumors occurring in *VCMsh2* mice at young ages have already acquired FSP mutations. These FSP mutations most likely represent early mutation events. FS mutations in *Xirp1* were not detected in MSI tumors of mice at the age of 7 months, but at a high frequency in tumors from older mice (Table 1).

VCMsh2 *Endogenous Adaptive Immunity Against Recurrent Frameshift Peptide Mutations*

To test whether *VCMsh2* mice have endogenous adaptive immunity directed against recurrent FSP neoantigens that could be boosted by vaccination, we performed splenocyte IFN-gamma ELISpot for Maz (FSP-1), Nacad (FSP-1), Senp6 (FSP-1), and Xirp1 (FSP-1) in 8- to 15-month-old *C57BL/6* and *VCMsh2* mice. This showed that, compared to *C57BL/6* control or OVA peptide-immunized mice (n = 5 and n = 6, respectively), *VCMsh2* splenocytes pulsed with Maz (FSP-1), Nacad (FSP-1), Senp6 (FSP-1), and Xirp1 (FSP-1) peptides in vitro had significantly higher numbers of activated IFN-gamma^{+} T cells (Figure 3*E*). Thus, similar to our previous findings that LS mutation carriers have endogenous adaptive immunity against recurrent FSP neoantigens,[23] *VCMsh2* mice have endogenous adaptive immunity against recurrent tumor FSP neoantigens.

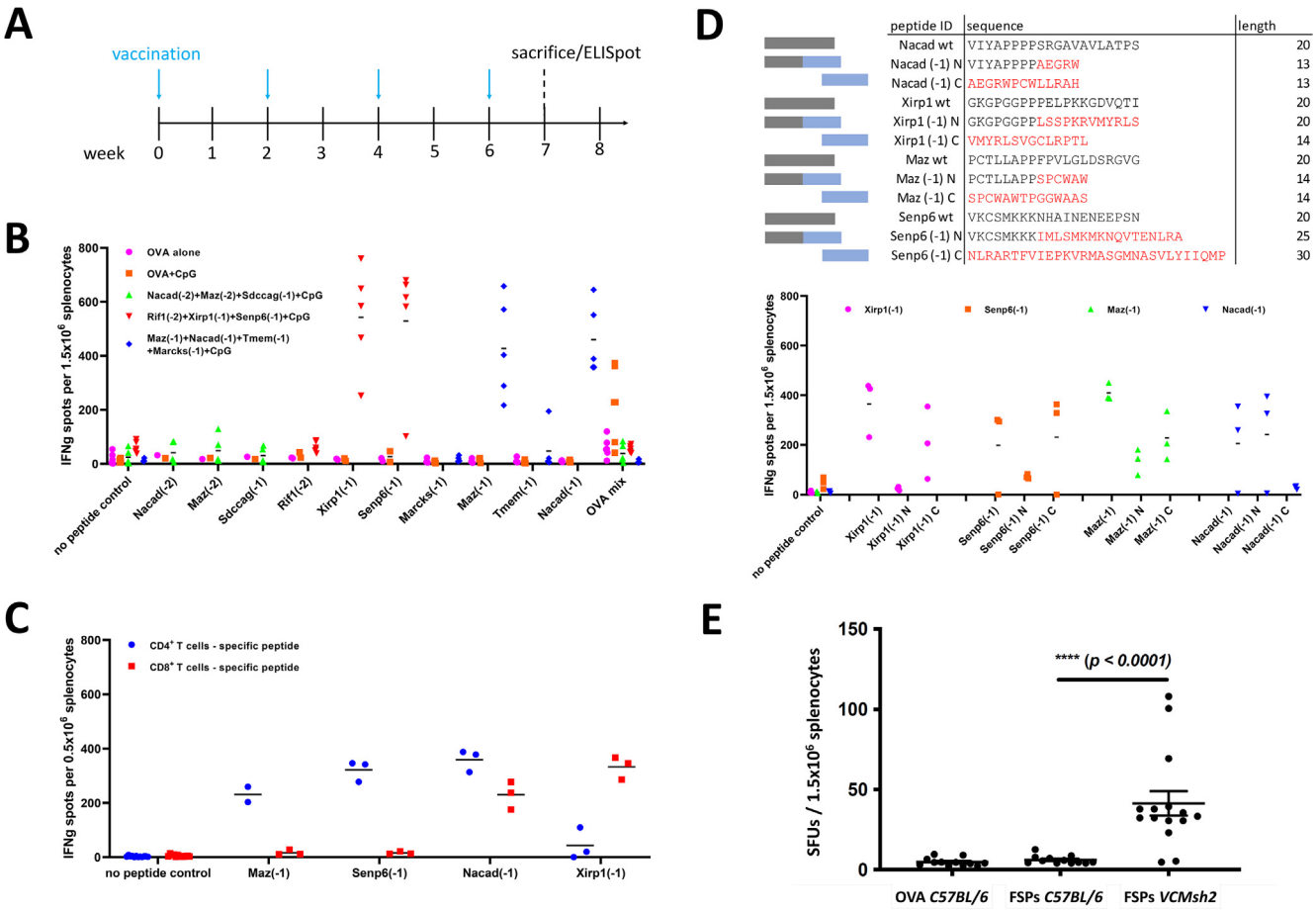

Figure 3. FSP immunogenicity. (*A*) FSP vaccination scheme of *C57BL/6* mice. FSP mixes or OVA mix (50 μg each) were injected subcutaneously biweekly 4 times using CpG ODN 1826 (20 μg) as an adjuvant. The vaccine schedule was chosen to ensure life-long robust FSP-specific immune responses, including a starting point in early adulthood and booster vaccinations after the initial priming phase. (*B*) IFN-gamma (IFN-g) ELISpot analysis. The mean number of spot-forming units (SFUs) for each mouse is shown for each peptide. OVA mix corresponds to the mixture of the OVA peptide CD4 and CD8 epitope, which was used as a control in this experimental setup. (*C*) CD4 and CD8 T cell responses against 4 FSPs. Mean SFU numbers are presented for each peptide. (*D*) Epitope mapping of immunogenic peptides. Wild-type peptides (*gray*), as well as FSPs with overlapping N/C-terminal sequences (*blue boxes*, *red* amino acids), were synthesized and immunogenicity for the regions where epitopes might be located was determined by IFN-gamma ELISpot. The mean number of SFUs per mouse are shown in the *graph*. (*E*) Endogenous FSP reactivity in Lynch mice. IFN-gamma ELISpot analysis. Each *dot* represents the number of SFUs of splenocytes per mouse. *VCMsh2* mice were pulsed with a mixture of 4 peptides (FSPs). *C57BL/6* (B6) mice pulsed with either FSPs or OVA peptide served as control. The median, interquartile range/SD, and significance level are indicated.

Optimization of Frameshift Peptide–Specific T Cell Activity With CpG Adjuvant

Several adjuvants recognized for their induction of CD8 T cell responses in mice were tested for compatibility with the FSP vaccine and for capacity to induce broad T cell responses across the panel of FSPs, including TLR9 agonists, STING agonists, and Montanide. Classes of novel adjuvant compounds have demonstrated the ability to activate type I IFN from dendritic cells, promote cross-presentation of soluble antigen to the MHC class I pathway, and have induced the development of tumor antigen–specific cytolytic T cells in murine models.[39–41] In addition, Montanide is a water-in-oil emulsion formulation that has a long track record of being paired with peptide vaccines in preclinical cancer vaccine investigations, as well as in clinical trials.[42,43]

To assess the FSP-specific T cell induction capability of these adjuvants, the 4-peptide FSP pool was combined with either the CpG-C ODN 2395, the CpG-B ODN 1826, the STING agonist 2′3′-cGAMP, or formulated with Montanide as an emulsion. The oil-in-water emulsion AddaVax was combined with the CpG ODNs and 2′3′-cGAMP to enhance adjuvant efficacy.[44] We observed robust T cell responses specific to the panel of FSPs as measured by ELISpot detection of IFN-gamma spot-forming units to Nacad (FSP-1), Xirp1 (FSP-1), Maz (FSP-1), and Senp6 (FSP-1) peptides with CpG/AddaVax adjuvant formulations (Supplementary Figure 4). However, 2′3′-cGAMP/AddaVax adjuvant yielded substantially lower T cell responses, while the Montanide formulation resulted in negligible spot-forming unit. Further investigation of the FSP vaccine in mice was conducted with CpG-B ODN 1826.

Reduced Tumor Burden and Increased Survival of Frameshift Peptide Vaccinated VCMsh2 *Lynch Syndrome Mice*

Next, we examined whether these 4 immunogenic FSPs might affect the survival of immunocompetent *VCMsh2* mice that develop small intestinal and colon tumors at the age of 6 months and have a mean life expectancy of about 14 months.[32] Six- to 8-week-old *VCMsh2* mice were either vaccinated with 4 FSPs or OVA control and CpG adjuvant and boosted 3× (Figure 4, Table 2). Tumor burden and survival analysis of vaccinated (n = 39) and control mice (n = 36) revealed that recurrent FSP neoantigen vaccination reduced tumor burden (mean control, 71.84 mg vs vaccinated, 47.26 mg, $P = .0024$, Mann-Whitney) and significantly increased survival (control median age, 256 days vs vaccinated, 327 days, control mean, 263 days vs vaccinated, 351 days; $P < .0001$, log-rank test).

Further Reduced Tumor Burden and Increased Survival of Naproxen-Treated and Frameshift Peptide–Vaccinated VCMsh2 *Lynch Syndrom Mice*

FSP vaccination was also tested in combination with ASA and NAP. *VCMsh2* mice were fed a diet including NAP (166 ppm) or ASA (400 ppm), as performed previously.[31] As expected, levels of prostaglandin E2 and other inflammatory prostaglandins PGD2 and PGF2a were significantly reduced in intestinal mucosa from these mice (Supplementary Figure 5). Similar to the previous findings,[31] both NAP and ASA exposure affected intestinal tumor development: NAP significantly reduced tumor burden and prolonged survival ($P = .0099$, Mann-Whitney and $P = .0005$, log-rank test), and ASA trended in this direction ($P = .23$ and $P = .081$ respectively, Figure 4). FSP vaccination prolonged survival more effectively compared with ASA ($P = .011$). The combination of FSP vaccination and NAP significantly prolonged survival compared to either intervention alone ($P = .0016$ and $P = .0005$, log-rank test, respectively) or ASA alone ($P = .0001$).

Quantification of Immune Cells in Manifest Tumors

In total, 22 tumor tissue specimens could be analyzed for immune cell infiltration (12 from the FSP vaccine group and 10 from the control group). Highest numbers of positively stained cells were observed for CD4-positive cells. Significantly elevated CD4-positive cell counts were recorded in tumors from the FSP vaccine group compared to tumors from the control group ($P = .048$). Similarly, CD8 T cell counts were significantly higher in the FSP vaccine vs control group ($P = .031$). No significant differences were observed for infiltrating Foxp3-positive or PD-1–positive cells (Figure 5).

NAP or ASA exposure did not have any significant effects on immune cell densities. Among tumors from vaccinated mice, CD8 and CD4 tumor infiltrating lymphocyte counts tended to be lower in animals exposed to NAP or ASA, although sample sizes were small.

RNA Sequencing Analysis Reveals Increased Immune Response in the VCMsh2 *Intestinal Tumor Microenvironment*

Next, to explore the molecular mechanisms of recurrent neoantigen vaccination and NSAID, we performed RNA sequencing using formalin-fixed, paraffin-embedded blocks from tumor and normal intestinal tissue from *VCMsh2* mice. As expected, this revealed substantial numbers of differentially regulated genes from FSP vaccination, NSAID cancer prevention, or their combination, in both tumors and normal intestinal tissue (Supplementary Figures 6 and 7, GSEA accession GSE175744). Only 1 differentially expressed gene, *Ptmap1/Ptma-ps1*, was shared among tumors from LS mice that were FSP vaccinated, treated with NSAIDs, or both (Supplementary Figure 6*B*). Ptmap1 is a poorly characterized gene that is ubiquitously expressed, encodes an open-reading frame with 76% amino acid identity to Ptma and may be an antagonist of Ptma. Reanalysis of previously published RNA sequencing data[45,46] showed that PTMA is up-regulated in LS patient CRCs and premalignant lesions compared to normal mucosa ($P = .00015$, Wilcoxon 2-tailed) (Supplementary Figure 6*C*), suggesting the PTMA/PTMAP1 axis as a potential novel candidate mechanism in LS CRC tumorigenesis. There were no significant changes in histologically normal intestinal mucosa for immune checkpoints PD1/PDL1, CTLA4, or LAG3 upon FSP vaccination or NSAID treatment (Supplementary Table 2). In terms of pathway analysis, as expected, *VCMsh2* intestinal tumors compared to adjacent normal tissue were characterized by up-regulation of WNT, NOTCH, and MYC signaling, epithelial to mesenchymal transition, angiogenesis, hypoxia, and stem cell and proliferation gene pathways, among others (Supplementary Figure 7). In addition, these tumors had down-regulation of Th1 IFN-gamma signaling and INF-alfa signaling, and up-regulation of Th2 $CD4^+$ T cell–mediated humoral B cell immunity. By comparison, tumors in FSP-vaccinated mice had notably increased IFN-gamma and p53 signaling, apoptosis, and reversal of IFN-alfa down-regulation. Thus, overall in the tumor microenvironment from FSP vaccinated mice, evidence for a relative up-regulation of Th1 compared to Th2 signaling pathways was detected (Supplementary Table 2 and Supplementary Figure 7). Interestingly, NSAIDs significantly down-regulated Th2 humoral immune response pathways, including B cell proliferation, B cell activation, and IgA production, thereby increasing the relative Th1:Th2 levels in the tumor microenvironment. In summary, both FSP vaccination and NSAIDs increased the relative Th1 vs Th2 immune response in the *VCMsh2* intestinal tumor microenvironment, although presumably via different mechanisms, while not significantly impacting immune checkpoint gene expression levels.

Discussion

LS is an important model to study immunopreventive cancer vaccination because tumors accumulate a predictable

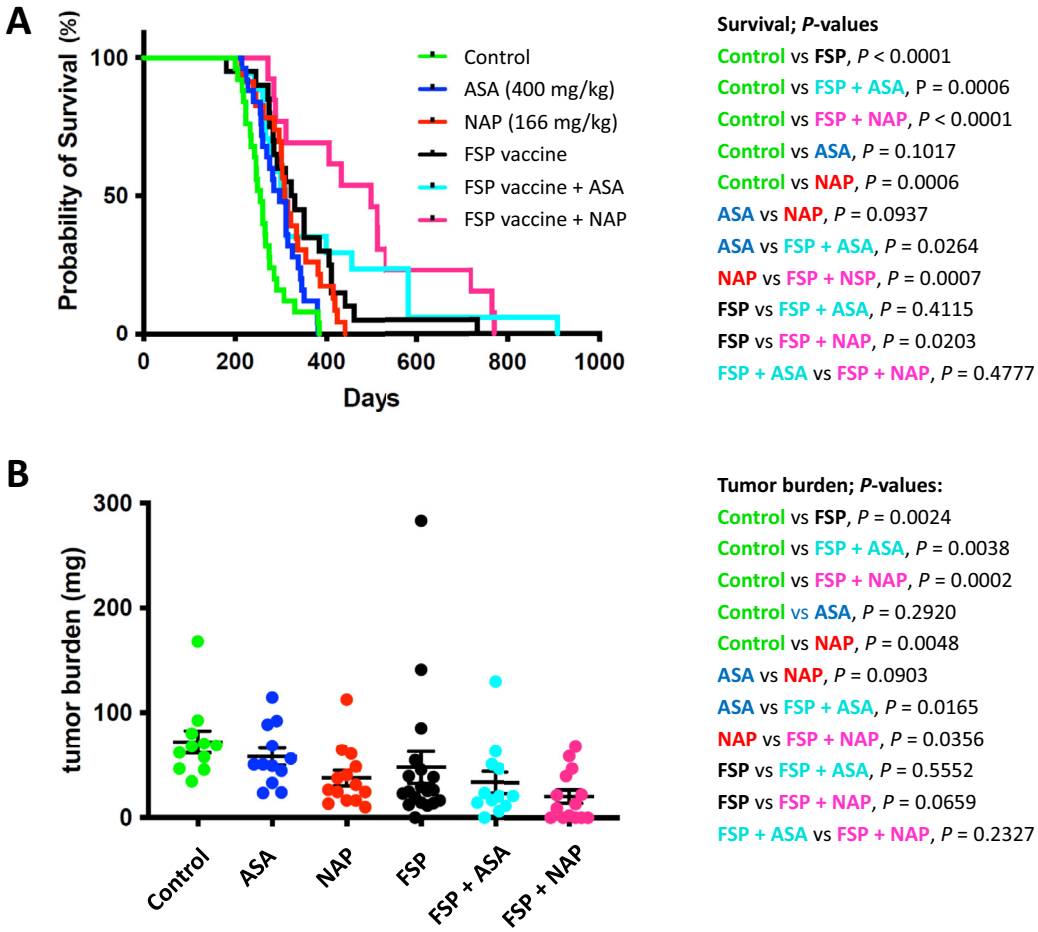

Figure 4. Cancer immunoprevention in Lynch mice. Reduced tumor burden from combination NSAID and recurrent FSP neoantigen vaccination. (*A*) Recurrent FSP neoantigen vaccination in combination with NSAID prolongs overall survival of *VCMsh2* mice. Kaplan-Meier survival curves of *VCMsh2* mice treated with control (untreated), ASA, NAP, FSP vaccine, FSP vaccine with ASA, or FSP vaccine with NAP, as described in the Materials and Methods. (*B*) FSP vaccination and combination with NSAID treatment decreases tumor burden in *VCMsh2* mice. *Scatter dot plot* representing tumor burden (sum of all intestinal tumor weights per mouse [mg]) per mouse in cohorts of control (untreated), treated with ASA, NAP, FSP vaccine, FSP vaccine plus ASA, or FSP vaccine plus NAP. Both *panels* present data updated from those originally presented in Supplementary Figure 3 of Reyes-Uribe et al,[30] here including a larger cohort of control and NAP-treated *VCMsh2* mice.

set of recurrent immunogenic neoantigens. This study provides the first robust evidence of tumor-preventive potential for a FSP neoantigen–based vaccine in a LS mouse model. Our experimental approach combined a series of methodical steps of in silico, in vitro, and in vivo analyses consisting of computational identification of murine cMNR candidates; molecular identification of shared tumor FS mutation targets; in silico prediction of FSP MHC binding motifs; FSP

Table 2. Tumor Burden and Survival in Different Treatment Groups

Variable	Control	ASA (400 mg/kg)	NAP (166 mg/kg)	FSP vaccine alone	FSP vaccine + ASA	FSP vaccine + NAP
Tumor burden, *mg*						
Mean	71.84	57.63	37.32	47.26	33.40	20.18
Sample size, n	11	12	14	19	12	14
Survival, *d*						
Mean	263.04	297.68	322.13	350.95	385.94	468
Median	256	297	309	327	311	464.5
Sample size, n	25	25	23	20	17	14

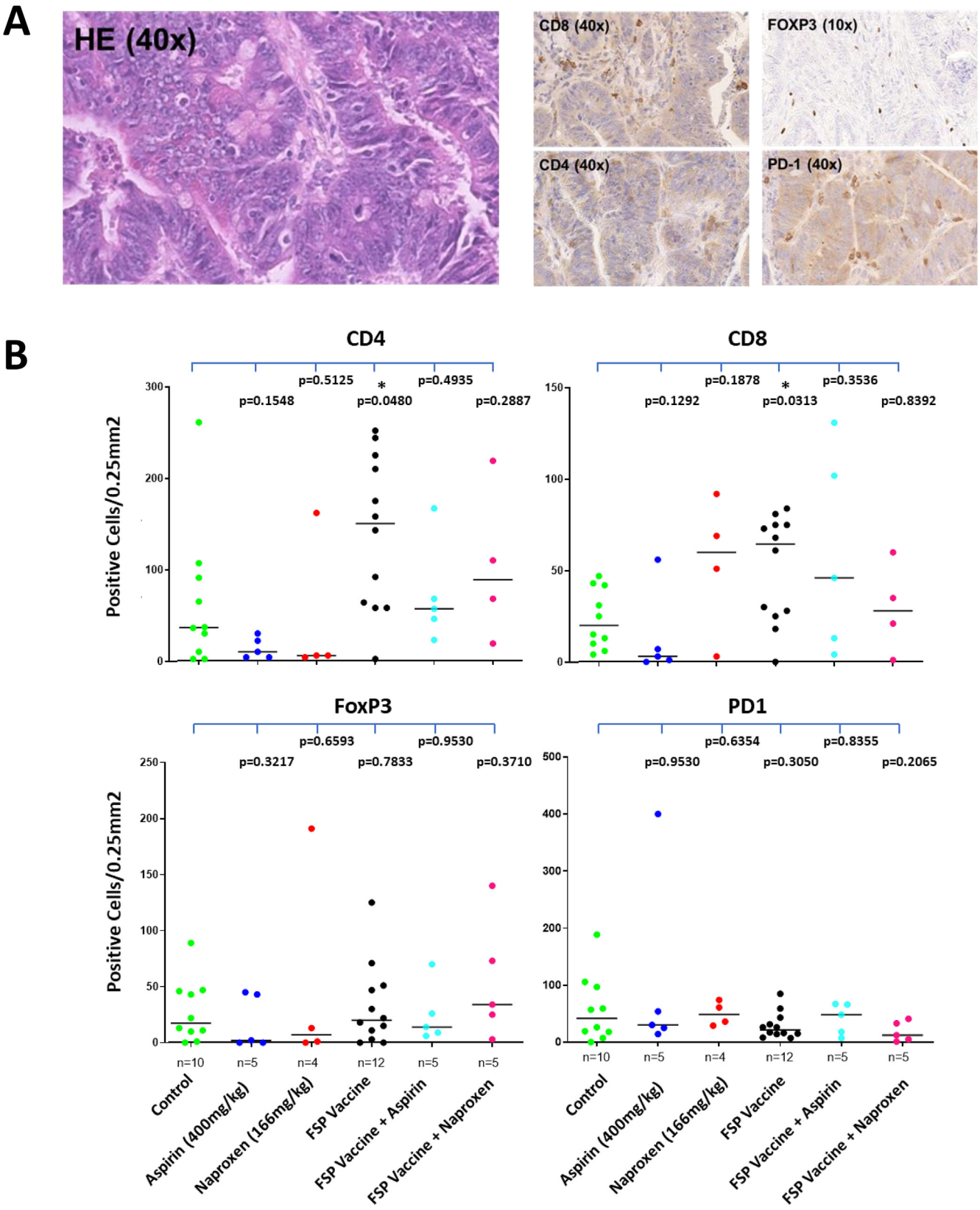

Figure 5. Quantitative evaluation of immune cell subtypes. (*A*) Representative immunohistochemistry stainings. HE, H&E. (*B*) Quantitative evaluation. Immune cell densities are shown for the antibodies detecting CD4, CD8, Foxp3, and PD-1. *Black lines* indicate median values. *P* values are provided for all comparisons.

immunogenicity testing; and integrated survival, tumor burden, and adaptive immune analyses in FSP-vaccinated LS mice.

As we have shown in a previous clinical phase I/II trial, FSP neoantigen vaccination is safe, nontoxic, and can elicit pronounced cellular and humoral immune response in advanced-stage MSI CRC patients.[24] However, data supporting the potential tumor-preventive effect of an FSP-based vaccine have been lacking. To evaluate FSP-based vaccination in the preventive setting, we used the *VCMsh2* LS mouse model[32] and compared survival of vaccinated mice with controls. We were able to demonstrate enhanced anti-FSP immunity, reduced tumor burden, and significantly prolonged survival of *VCMsh2* mice receiving the FSP vaccine compared to unvaccinated mice.

The *VCMsh2* model recapitulates human LS, as these mice develop MMRD intestinal tumors. These mice have an intestinal-specific exon 12 deletion of the *Msh2* gene *by Villin-Cre* and inactivate MMR functions similar to MMRD found in patients with LS. As an additional advantage, and in contrast to constitutive MMR-knockout models, the conditional ablation of *Msh2* in *VCMsh2* mice promotes tumor development specifically in the intestinal epithelium. This model also provides benefits in terms of NSAID cancer prevention studies because dietary ASA can suppress tumorigenesis in these mice similar to the tumor-protective effect of long-term ASA observed in humans (CAPP2 trial of patients with LS[28]). Despite these similarities, tumor localization appears to be different because *VCMsh2* mice usually develop tumors in the small intestine, whereas colonic tumors predominate in patients with LS. Also, a direct transfer of human FSPs to the murine model is not feasible due to genomic differences, in terms of the location of cMNRs in coding regions and the nucleotide sequence of the respective genes, and differences in the MHC molecules responsible for antigen presentation. Therefore, we established a comprehensive database of murine cMNRs, providing a unique source of murine candidate genes and derived FSPs.

Using this genome-wide computational approach, we were able to select 4 candidate FSPs, which are shared by different murine MSI intestinal tumors, and validated their immunogenicity in vivo. The 4 FSPs Nacad (FSP-1), Maz (FSP-1), Senp6 (FSP-1), and Xirp1 (FSP-1) generated cellular and humoral immune responses in naïve mice. ELISpot analyses showed CD8 T cell–specific response for Xirp1 (FSP-1), a mixed CD4/CD8 T cell response for Nacad (FSP-1), and a CD4 T cell–specific response for Maz1 (FSP-1) and Senp6 (FSP-1), partially overlapping with in silico prediction of MHC binding motifs. Three of these 4 FSPs also elicited humoral immune responses, which were only absent for Xirp1 (FSP-1), consistent with the observed restriction of cellular immune responses to CD8, but not CD4 T cells, which play a major role in mediation of humoral immune responses. When analyzing immune cell infiltration of tumors in *VCMsh2* mice receiving the FSP vaccine, we observed a significantly elevated density of CD4-positive and CD8-positive T cells in tumors compared to non-vaccinated control mice; densities for CD4-positive T cells were generally higher than the density of CD8-positive T cells. These findings are consistent with a predominance of CD4 responses triggered by FSP vaccination, as observed in human patients with MSI CRC who were vaccinated with a trivalent FSP vaccine.[24] Previously, CD4-positive T cell responses were shown to be predominant and associated with clinical response in "personalized" melanoma and glioblastoma patient neoantigen and tumor-associated antigen vaccine trials.[47–49] Thus, our findings support important roles for CD4-positive (in addition to CD8-positive) T cells in durable clinical responses to tumor vaccines.

The fact that cMNR mutations affecting the genes *Nacad*, *Maz*, *Senp6*, and *Xirp1* were found to be recurrent across tumors may suggest a functional role of these mutations as drivers of tumor development. Although some evidence of involvement in tumor development exists for the genes *Maz* and *Senp6*,[50–53] very limited functional data are available for *Nacad* and *Xirp1*. Thus, further studies are required to elucidate a potential functional contribution of these mutations to MSI tumor progression.

Although, as outlined above, the precise amino acid sequence differs between murine and human FSP neoantigens, the observed immunopreventive effects support the hypothesis that vaccination with shared FSP neoantigens may be a powerful approach for cancer prevention in LS. In particular, it is notable that vaccination with only a limited number of FSPs combined with relatively low dose of NAP significantly delayed tumor formation and prolonged overall survival in LS mice, providing a rational approach for combination cancer- and immuno-prevention.

Our study addresses, for the first time to our knowledge, the important question of whether FSP vaccination and NSAIDs are synergistic or antagonistic in LS cancer prevention. The increased survival and reduced tumor burden of mice receiving both FSP vaccination and NSAID treatment is consistent with a role for combined chemo- and immunoprevention to reduce tumor burden in a practical manner. Our observations suggest that the combination of FSP vaccination and NSAID treatment is beneficial, possibly by partially complementary mechanisms, which need to be elucidated in future studies.

By analyzing transcriptomic pathways altered by FSP vaccination and NSAIDs, we identified a differentially expressed gene, *Ptmap1*, that was differentially regulated in tumors from LS mice that were FSP vaccinated, treated with NSAIDs, and then further up-regulated by combined treatment. PTMA is a nuclear oncoprotein transcription factor that is up-regulated in solid tumors, including CRC, and is functionally associated with CRC poor prognosis.[54] PTMAP1 overall remains poorly characterized. Because PTMAP1 is highly homologous to PTMA at the protein level, it may antagonize PTMA oncogenic transcriptional program functions. However, these findings are exploratory and further studies are needed to assess the mechanistic role of the PTMA/PTMAP1 axis in LS CRC tumorigenesis.

In terms of transcriptomic pathways, both FSP vaccination and NSAIDs increased the relative Th1 vs Th2 T cell immune response in the *VCMsh2* intestinal tumor microenvironment, while not significantly impacting critical immune checkpoint gene expression levels, which for PD-1 was

confirmed by quantitative immunohistochemistry (Figure 5). Thus, elevated Th1 T cell activation in the tumor microenvironment is the most likely immune surveillance mechanism to account for the observed reduced tumor burden in FSP-vaccinated, NSAID-treated, and combination-treated mice.

This study has several limitations. Our study was conducted in mice that have defined MHC molecules, whereas LS patients have much broader HLA (class I and class II MHC) diversity. It remains to be demonstrated whether a broader spectrum of shared FSPs in combination with other cancer prevention approaches might represent an even more effective strategy to prevent LS tumors in patients with greater HLA diversity. Although CpG1826 showed best results among the 4 adjuvants screened in LS mice, it is unclear whether alternative adjuvants might be more effective for FSP vaccination in human LS patients. In the same context, the most effective boosting regimen is still unknown. Additional preclinical studies addressing these questions will be required before large-scale LS immunoprevention trials are carried out.

In summary, our results strongly support the concept of FSP neoantigen vaccination as a promising strategy for immunoprevention of intestinal MMRD tumors, particularly in the setting of LS. We provided the first evidence that vaccination with a small number of shared FSP neoantigens alone effectively delays formation of naturally occurring tumors and prolonged survival in an LS mouse model. Furthermore, as NSAID use is the current choice of care for patients with LS, we showed that this benefit can be enhanced significantly in a cooperative manner by combining FSP vaccination with NSAID treatment. Clinical translation of this concept of neoantigen-based tumor prevention is encouraging, and our studies support further preclinical and clinical studies to translate this benefit for LS immunoprevention.

Supplementary Material

Note: To access the supplementary material accompanying this article, visit the online version of *Gastroenterology* at www.gastrojournal.org, and at http://doi.org/10.1053/j.gastro.2021.06.073.

References

1. Ionov Y, Peinado MA, Malkhosyan S, et al. Ubiquitous somatic mutations in simple repeated sequences reveal a new mechanism for colonic carcinogenesis. Nature 1993;363:558–561.
2. Thibodeau SN, Bren G, Schaid D. Microsatellite instability in cancer of the proximal colon. Science 1993; 260:816–819.
3. Kloor M, von Knebel Doeberitz M. The immune biology of microsatellite-unstable cancer. Trends Cancer 2016; 2:121–131.
4. **Markowitz S, Wang J, Myeroff L**, et al. Inactivation of the type II TGF-beta receptor in colon cancer cells with microsatellite instability. Science 1995;268:1336–1338.
5. Woerner SM, Yuan YP, Benner A, et al. SelTarbase, a database of human mononucleotide-microsatellite mutations and their potential impact to tumorigenesis and immunology. Nucleic Acids Res 2010;38:D682–D689.
6. **Jonchere V, Marisa L, Greene M**, et al. Identification of positively and negatively selected driver gene mutations associated with colorectal cancer with microsatellite instability. Cell Mol Gastroenterol Hepatol 2018;6:277–300.
7. Colas C, Coulet F, Svrcek M, et al. Lynch or not Lynch? Is that always a question? Adv Cancer Res 2012; 113:121–166.
8. **Latham A, Srinivasan P**, Kemel Y, et al. Microsatellite instability is associated with the presence of Lynch syndrome pan-cancer. J Clin Oncol 2019;37:286–295.
9. Win AK, Jenkins MA, Dowty JG, et al. Prevalence and penetrance of major genes and polygenes for colorectal cancer. Cancer Epidemiol Biomarkers Prev 2017; 26:404–412.
10. Haraldsdottir S, Rafnar T, Frankel WL, et al. Comprehensive population-wide analysis of Lynch syndrome in Iceland reveals founder mutations in MSH6 and PMS2. Nat Commun 2017;8:14755.
11. Moller P, Seppala TT, Bernstein I, et al. Cancer risk and survival in path_MMR carriers by gene and gender up to 75 years of age: a report from the Prospective Lynch Syndrome Database. Gut 2018;67:1306–1316.
12. Seppala T, Pylvanainen K, Evans DG, et al. Colorectal cancer incidence in path_MLH1 carriers subjected to different follow-up protocols: a Prospective Lynch Syndrome Database report. Hered Cancer Clin Pract 2017; 15:18.
13. Fishel R, Lescoe MK, Rao MR, et al. The human mutator gene homolog MSH2 and its association with hereditary nonpolyposis colon cancer. Cell 1993;75:1027–1038.
14. Jasperson KW, Tuohy TM, Neklason DW, et al. Hereditary and familial colon cancer. Gastroenterology 2010; 138:2044–2058.
15. Hemminki A, Peltomaki P, Mecklin JP, et al. Loss of the wild type MLH1 gene is a feature of hereditary nonpolyposis colorectal cancer. Nat Genet 1994;8:405–410.
16. Veigl ML, Kasturi L, Olechnowicz J, et al. Biallelic inactivation of hMLH1 by epigenetic gene silencing, a novel mechanism causing human MSI cancers. Proc Natl Acad Sci U S A 1998;95:8698–8702.
17. Dolcetti R, Viel A, Doglioni C, et al. High prevalence of activated intraepithelial cytotoxic T lymphocytes and increased neoplastic cell apoptosis in colorectal carcinomas with microsatellite instability. Am J Pathol 1999; 154:1805–1813.
18. **Buckowitz A, Knaebel HP**, Benner A, et al. Microsatellite instability in colorectal cancer is associated with local lymphocyte infiltration and low frequency of distant metastases. Br J Cancer 2005;92:1746–1753.
19. **Giannakis M, Mu XJ, Shukla SA**, et al. Genomic correlates of immune-cell infiltrates in colorectal carcinoma. Cell Rep 2016;17:1206.
20. **Mandal R, Samstein RM, Lee KW**, et al. Genetic diversity of tumors with mismatch repair deficiency

influences anti-PD-1 immunotherapy response. Science 2019;364:485–491.
21. **Linnebacher M, Gebert J**, Rudy W, et al. Frameshift peptide-derived T-cell epitopes: a source of novel tumor-specific antigens. Int J Cancer 2001;93:6–11.
22. Saeterdal I, Bjorheim J, Lislerud K, et al. Frameshift-mutation-derived peptides as tumor-specific antigens in inherited and spontaneous colorectal cancer. Proc Natl Acad Sci U S A 2001;98:13255–13260.
23. Schwitalle Y, Kloor M, Eiermann S, et al. Immune response against frameshift-induced neopeptides in HNPCC patients and healthy HNPCC mutation carriers. Gastroenterology 2008;134:988–997.
24. Kloor M, Reuschenbach M, Pauligk C, et al. A frameshift peptide neoantigen-based vaccine for mismatch repair-deficient cancers: a phase I/IIa clinical trial. Clin Cancer Res 2020;26:4503–4510.
25. Burn J, Gerdes AM, Macrae F, et al. Long-term effect of aspirin on cancer risk in carriers of hereditary colorectal cancer: an analysis from the CAPP2 randomised controlled trial. Lancet 2011;378:2081–2087.
26. Wang D, Dubois RN. Eicosanoids and cancer. Nat Rev Cancer 2010;10:181–193.
27. **Roulis M, Kaklamanos A**, Schernthanner M, et al. Paracrine orchestration of intestinal tumorigenesis by a mesenchymal niche. Nature 2020;580:524–529.
28. Burn J, Sheth H, Elliott F, et al. Cancer prevention with aspirin in hereditary colorectal cancer (Lynch syndrome), 10-year follow-up and registry-based 20-year data in the CAPP2 study: a double-blind, randomised, placebo-controlled trial. Lancet 2020;395:1855–1863.
29. **McNeil JJ, Nelson MR**, Woods RL, et al. Effect of aspirin on all-cause mortality in the healthy elderly. N Engl J Med 2018;379:1519–1528.
30. Reyes-Uribe L, Wu W, Gelincik O, et al. Naproxen chemoprevention promotes immune activation in Lynch syndrome colorectal mucosa. Gut 2021;70:555–566.
31. Martin-Lopez J, Gasparini P, Coombes K, et al. Mutation of TGFbeta-RII eliminates NSAID cancer chemoprevention. Oncotarget 2018;9:12554–12561.
32. **Kucherlapati MH, Lee K, Nguyen AA**, et al. An Msh2 conditional knockout mouse for studying intestinal cancer and testing anticancer agents. Gastroenterology 2010;138:993–1002.e1.
33. Heyer J, Yang K, Lipkin M, et al. Mouse models for colorectal cancer. Oncogene 1999;18:5325–5333.
34. Woerner SM, Tosti E, Yuan YP, et al. Detection of coding microsatellite frameshift mutations in DNA mismatch repair-deficient mouse intestinal tumors. Mol Carcinog 2015;54:1376–1386.
35. Woerner SM, Kloor M, von Knebel Doeberitz M, et al. Microsatellite instability in the development of DNA mismatch repair deficient tumors. Cancer Biomark 2006; 2:69–86.
36. **Woerner SM, Kloor M**, Mueller A, et al. Microsatellite instability of selective target genes in HNPCC-associated colon adenomas. Oncogene 2005;24:2525–2535.
37. Kabbarah O, Mallon MA, Pfeifer JD, et al. A panel of repeat markers for detection of microsatellite instability in murine tumors. Mol Carcinog 2003;38:155–159.
38. Bankhead P, Loughrey MB, Fernandez JA, et al. QuPath: open source software for digital pathology image analysis. Sci Rep 2017;7:16878.
39. **Su T, Zhang Y**, Valerie K, et al. STING activation in cancer immunotherapy. Theranostics 2019;9:7759–7771.
40. **Shirota H, Tross D**, Klinman DM. CpG oligonucleotides as cancer vaccine adjuvants. Vaccines (Basel) 2015; 3:390–407.
41. Gogoi H, Mansouri S, Jin L. The age of cyclic dinucleotide vaccine adjuvants. Vaccines (Basel) 2020;8:453.
42. Hailemichael Y, Dai Z, Jaffarzad N, et al. Persistent antigen at vaccination sites induces tumor-specific CD8(+) T cell sequestration, dysfunction and deletion. Nat Med 2013;19:465–472.
43. Iwasa S, Yamada Y, Heike Y, et al. Phase I study of a new cancer vaccine of ten mixed peptides for advanced cancer patients. Cancer Sci 2016;107:590–600.
44. **Maynard SK, Marshall JD**, MacGill RS, et al. Vaccination with synthetic long peptide formulated with CpG in an oil-in-water emulsion induces robust E7-specific CD8 T cell responses and TC-1 tumor eradication. BMC Cancer 2019;19:540.
45. Bommi PV, Bowen CM, Reyes-Uribe L, et al. The transcriptomic landscape of mismatch repair-deficient intestinal stem cells. Cancer Res 2021;81:2760–2773.
46. Chang K, Taggart MW, Reyes-Uribe L, et al. Immune profiling of premalignant lesions in patients with lynch syndrome. JAMA Oncol 2018;4:1085–1092.
47. **Keskin DB, Anandappa AJ, Sun J**, et al. Neoantigen vaccine generates intratumoral T cell responses in phase Ib glioblastoma trial. Nature 2019;565:234–239.
48. Sahin U, Oehm P, Derhovanessian E, et al. An RNA vaccine drives immunity in checkpoint-inhibitor-treated melanoma. Nature 2020;585:107–112.
49. Sahin U, Derhovanessian E, Miller M, et al. Personalized RNA mutanome vaccines mobilize poly-specific therapeutic immunity against cancer. Nature 2017;547:222–226.
50. Chen T, Xue H, Lin R, et al. MiR-34c and PlncRNA1 mediated the function of intestinal epithelial barrier by regulating tight junction proteins in inflammatory bowel disease. Biochem Biophys Res Commun 2017; 486:6–13.
51. **Yu ZH, Lun SM**, He R, et al. Dual function of MAZ mediated by FOXF2 in basal-like breast cancer: promotion of proliferation and suppression of progression. Cancer Lett 2017;402:142–152.
52. Bologna S, Altmannova V, Valtorta E, et al. Sumoylation regulates EXO1 stability and processing of DNA damage. Cell Cycle 2015;14:2439–2450.
53. Tosti E, Katakowski JA, Schaetzlein S, et al. Evolutionarily conserved genetic interactions with budding and fission yeast MutS identify orthologous relationships in mismatch repair-deficient cancer cells. Genome Med 2014;6:68.
54. Zhang M, Cui F, Lu S, et al. Increased expression of prothymosin-alpha, independently or combined with TP53, correlates with poor prognosis in colorectal cancer. Int J Clin Exp Pathol 2014;7:4867–4876.

Author names in bold designate shared co-first authorship.

Received October 2, 2020. Accepted June 28, 2021.

Correspondence
Address correspondence to: Johannes Gebert, PhD, Department of Applied Tumor Biology, Institute of Pathology, Heidelberg University Hospital, Im Neuenheimer Feld 224, 69120 Heidelberg, Germany. e-mail: johannes.gebert@med.uni-heidelberg.de; Magnus von Knebel Doeberitz, MD, Department of Applied Tumor Biology, Institute of Pathology, Heidelberg University Hospital, Im Neuenheimer Feld 224, 69120 Heidelberg, Germany. e-mail: magnus.knebel-doeberitz@med.uni-heidelberg.de; Steven M. Lipkin, MD, Weill Cornell Medical College, New York, 10021 New York. e-mail: stl2012@med.cornell.edu; or Matthias Kloor, MD, Department of Applied Tumor Biology, Institute of Pathology, Heidelberg University Hospital, Im Neuenheimer Feld 224, 69120 Heidelberg, Germany. e-mail: matthias.kloor@med.uni-heidelberg.de.

CRediT Authorship Contributions
Johannes Gebert, PhD (Conceptualization: Equal; Data curation: Supporting; Formal analysis: Equal; Funding acquisition: Equal; Project administration: Equal; Writing – original draft: Lead; Writing – review & editing: Equal).

Gelincik Ozkan, PhD (Data curation: Supporting; Investigation: Equal; Methodology: Supporting; Writing – review & editing: Supporting).

Ozcan-Wahlbrink Mine, PhD (Data curation: Supporting; Investigation: Equal; Methodology: Supporting; Writing – review & editing: Supporting).

Jason Marshall, PhD (Data curation: Supporting; Investigation: Supporting; Methodology: Supporting; Writing – review & editing: Supporting).

Alejandro Hernandez Sanchez, MS (Investigation: Supporting; Visualization: Supporting; Writing – review & editing: Supporting).

Katharina Urban, PhD (Investigation: Supporting; Writing – review & editing: Supporting).

Mark Long, PhD (Formal analysis: Supporting; Resources: Supporting; Software: Supporting; Writing – review & editing: Supporting).

Eduardo Cortes, MS (Formal analysis: Supporting; Resources: Supporting; Software: Supporting; Writing – review & editing: Supporting).

Elena Tosti, PhD (Methodology: Supporting; Resources: Supporting; Writing – review & editing: Supporting).

Eva Katzenmaier, PhD (Methodology: Supporting; Resources: Supporting; Writing – review & editing: Supporting).

Yurong Song, PhD (Investigation: Supporting; Methodology: Supporting; Writing – review & editing: Supporting).

Ali Elsaadi, MD (Investigation: Supporting; Methodology: Supporting; Writing – review & editing: Supporting).

Nan Deng, PhD (Formal analysis: Supporting; Resources: Supporting; Software: Supporting; Writing – review & editing: Supporting).

Eduardo Vilar, MD (Data curation: Supporting; Formal analysis: Equal; Writing – review & editing: Supporting).

Vera Fuchs, BSc (Investigation: Supporting; Writing – review & editing: Supporting).

Nina Nelius, BSc (Investigation: Supporting; Writing – review & editing: Supporting).

Yan Yuan, PhD (Formal analysis: Supporting; Resources: Supporting; Software: Lead; Writing – review & editing: Supporting).

Aysel Ahadova, PhD (Investigation: Supporting; Visualization: Supporting; Writing – review & editing: Supporting).

Shizuko Sei, MD (Conceptualization: Supporting; Data curation: Supporting; Project administration: Supporting; Writing – review & editing: Supporting).

Robert H Shoemaker, PhD (Data curation: Supporting; Project administration: Supporting; Writing – review & editing: Supporting).

Asad Umar, DVM, PhD (Conceptualization: Supporting; Data curation: Supporting; Project administration: Supporting; Writing – review & editing: Supporting).

Lei Wei, PhD (Formal analysis: Supporting; Resources: Supporting; Software: Supporting; Writing – review & editing: Supporting).

Song Liu, PhD (Formal analysis: Supporting; Resources: Supporting; Software: Supporting; Writing – review & editing: Supporting).

Peer Bork, PhD (Resources: Supporting; Software: Lead; Writing – review & editing: Supporting).

Winfried Edelmann, PhD (Methodology: Supporting; Resources: Equal; Writing – review & editing: Supporting).

Magnus von Knebel Doeberitz, MD (Conceptualization: Equal; Funding acquisition: Supporting; Project administration: Equal; Supervision: Equal; Writing – original draft: Supporting; Writing – review & editing: Supporting).

Steven Lipkin, MD (Conceptualization: Supporting; Data curation: Supporting; Formal analysis: Equal; Funding acquisition: Equal; Project administration: Equal; Supervision: Equal; Writing – original draft: Supporting; Writing – review & editing: Equal).

Matthias Kloor, MD (Conceptualization: Equal; Data curation: Supporting; Formal analysis: Equal; Funding acquisition: Equal; Project administration: Equal; Writing – original draft: Supporting; Writing – review & editing: Equal).

Conflicts of interest
This author discloses the following: Eduardo Vilar has a consulting or advisory role with Janssen Research and Development and Recursion Pharma. He has received research support from Janssen Research and Development. The remaining authors disclose no conflicts.

Funding
This work was supported by a grant from the Deutsche Forschungsgemeinschaft (GE 592-9/1) and a contract from the PREVENT Preclinical Development Program, Division Cancer Prevention, National Cancer Institute (HHSN2612015000391), U01CA233056 and U24CA232979. This work was supported by grant R01 CA219463, a gift from the Feinberg Family Foundation, the MD Anderson Colorectal Cancer Moonshot to Eduardo Vilar; and P30 CA016672 (US National Institutes of Health/National Cancer Institute) to the University of Texas MD Anderson Cancer Center Core Support Grant.

Data transparency statement
All relevant data are contained in the manuscript or the Supplementary Material. Transcript profiling data are available under the following link: https://www.ncbi.nlm.nih.gov/geo/query/acc.cgi?acc=GSE175744

Supplementary Methods

Detailed Protocol Descriptions

DNA/RNA isolation of *VCMsh2* mouse tumors from formalin-fixed, paraffin-embedded tissues. For determination of cMNR mutation frequency, formalin-fixed paraffin-embedded (FFPE) tissue blocks were generated from *VCMsh2* mice after they had developed intestinal tumors at the age of 7–15 months (n = 25). Each tissue section contained normal mucosa and tumor tissue. To ensure enrichment of tumor cells (>80%), tissue sections were microdissected. Sufficient amounts of DNA and RNA were obtained by pooling microdissected tissues from several consecutive sections. DNA and RNA from matched normal/tumor tissues were isolated using the QIAmpDNA FFPE Tissue and the RNeasy Mini Kits (Qiagen).

Coding mononucleotide repeat mutation analysis. Oligonucleotide primers for the amplification of cMNR sequences were designed using the search tool Primer 3 (http://www.broadinstitute.org, http://bioinfo.ut.ee/primer3/). Other considerations for primer design included considering the requirement for small amplicon size (100–140 bp) required for robust amplification from genomic DNA of murine FFPE tissues. One primer of each primer set carried a fluorescent (fluorescein isothiocyanate) label at the 5′-end. FS mutations were identified by polymerase chain reaction–based DNA fragment length analysis. Instability was scored qualitatively, if novel peaks were obtained in the tumor compared to normal tissue, or quantitatively by processing extracted peak height profiles by a custom R algorithm.

Preparation of peptides with CpG adjuvant for vaccination of *C57Bl/6* mice. For preparation of the vaccine formulations, lyophilized peptides (OVA or equimolar concentrations of Senp6, Xirp1, Maz, and Nacad) were resuspended in 20% dimethyl sulfoxide containing distilled phosphate-buffered saline to achieve a final concentration of 5 mg/mL and stored at –80°C. Lyophilized OVA peptide was resuspended in sterile water to achieve a final concentration of 4 mg/mL each. Then, 5 μL of OVA 257–264 (4 mg/mL) was mixed with 5 μL of OVA 323–339 to achieve a final concentration of 2 mg/mL each and stored at –80°C. The lyophilized adjuvant (CpG ODN 1826) was resuspended in sterile water to achieve a final concentration of 2 mg/mL and stored at –80°C.

Adjuvant optimization in wild-type *C57BL/6* mice. FSPs (OVA or Senp6 [FSP-1], Xirp1 [FSP-1], Maz [FSP-1], and Nacad [FSP-1]) were synthesized at Pierce (Thermo Fisher), received with certificates of analysis, and stored lyophilized at –80°C; or by GenScript at 90% purity and solubilized as a pool at 5 mg/mL each peptide in dimethyl sulfoxide. CpG-B ODN 1826, CpG-C ODN 2395, 2′3′-cGAMP, and AddaVax were all purchased from InvivoGen. CpG ODNs and 2′3′-cGAMP were first mixed with AddaVax and then combined with FSPs to prepare vaccines in which 100-μL dose volume per mouse contained 50 μg each of 4 FSPs, 50% v/v AddaVax, and either 20 μg 1826, 20 μg 2395, or 15 μg 2′3′-cGAMP. FSPs were also solubilized in 1× phosphate-buffered saline and combined with Montanide ISA-720 (Seppic) in a 30:70 v/v ratio. Syringes (3 cc) were separately loaded with the aqueous peptide phase or with Montanide and then connected with an I-connector. Emulsion was generated by cycling total volume of both phases back and forth between the 2 syringes 20 times, 8 seconds per cycle, and then 60 times, 2 seconds per cycle, until the emulsion adopted a creamy viscous appearance. After briefly mixing by vortex, vaccines were administered to mice. Ten-week-old female *C57BL/6* mice (Charles River) were randomized into groups of 8 animals and immunized on study days 0, 14, and 28 (2-week intervals). Mice were injected subcutaneously in alternate flanks with 100-μL dose volumes. Spleens were harvested on day 42 and the obtained cell suspensions were analyzed by IFN-gamma ELISpot, as described in Supplementary Methods.

Interferon-gamma enzyme-linked immunosorbent spot assay. Spleens were harvested and dissociated using the GentleMACS Dissociator (Miltenyi). Cell suspensions were subsequently washed with Hank's balanced salt solution (Gibco) + 5% fetal bovine serum (Gibco), lysed to remove red blood cells with ACK Lysing Buffer (Thermo-Fisher), and filtered through 70-μm strainers (BD Biosciences). Cells were counted with the Vi-Cell analyzer (Beckman Coulter) and resuspended in RPMI-1640 (Thermo-Fisher) + 10% fetal bovine serum and resuspended in culture medium (RPMI-1640 + 10% fetal bovine serum) at 5e6/mL. The R&D Systems mouse IFN-gamma ELISpot assay was performed according to the manufacturer's specifications. After blocking plates with culture media, stimulants were added to plates, including 5 μg/mL individual FSP peptides (synthesized by GenScript) and OVA SIINFEKL peptide (InvivoGen). Lastly, 2.5^{e5} splenocytes were added per well in triplicate in a volume of 50 μL and plates were incubated in a 37°C, 5% CO_2 incubator for 42–48 hours. ELISpot plates were then developed according to the manufacturer's protocol. Plates were washed with the BioTek EL405 plate washer. After a developing step, plates were air-dried for 24 hours and then imaged and spots counted on an ImmunoSpot Analyzer (C.T.L.) using ImmunoCapture software.

Enzyme-linked immunosorbent assay of frameshift peptide humoral immunogenicity. After sacrificing, whole blood was collected from mice via cardiac puncture and centrifuged to obtain serum for enzyme-linked immunosorbent assay (ELISA) analysis. Ninety-six-well ELISA plates were coated with the peptide of interest, and serially diluted mouse sera were added into the wells in quadruplicates. The optical density of the ELISA reaction was measured at 405 nm in an ELISA reader with a reference wavelength of 620 nm. Reactions significantly above background after subtraction of twice the SE of the peptide only background and no-peptide antigen only control values were regarded as positive. Titration was performed to quantify the amounts of neoantigen-specific IgG antibodies in mouse sera for all 4 peptides.

Murine intestinal tumor analysis. For intestinal tumor analysis, a general survey was performed of mice for gross pathology of any abdominal or thoracic cavity organ. Euthanized mice were dissected and small intestines and colons were washed in ice-cold distilled phosphate-buffered saline. Normal intestinal tissue and adenomas were dissected. Lesions were then counted, dissected out, weighed, and either flash frozen in Optimal Cutting Temperature medium for RNA or embedded in paraffin for H&E for further histologic analysis by a pathologist. All tumors were confirmed by histopathological evaluation. For each mouse, tumor multiplicity, weight, and tumor burden (sum of tumor weights per mouse) data were included in the analysis. For all mice, age at the time of euthanasia was recorded for survival analysis. Mice that died or were euthanized due to unrelated causes (eg, dermatitis) were excluded from survival analysis. DNA/RNA isolation was carried out using QiaAmp DNA and RNeasy RNA Isolation kit, respectively, in preparation for follow-up studies in the future.

Immunohistochemistry staining. For quantification of tumor infiltrating lymphocyte densities, tissue sections were deparaffinized and rehydrated by submerging for 5 minutes in 3 different 100% xylene baths, two 100% ethanol baths, one 96% ethanol bath, and one 70% ethanol bath, and 1 deionized water bath. Antigen retrieval was carried out by microwaving the slides 3 times for 10 minutes at 560 watts, either in a 10 mM citric acid monohydrate solution at pH 6.0 (for CD3) or in a Tris-EDTA solution at pH 8.5 (for CD4, CD8, Foxp3, and PD-1). Endogenous peroxidase was quenched by treating the slides with 0.6% hydrogen peroxide in methanol for 20 minutes. After blocking the nonspecific binding with 10% horse serum for 30 minutes, the slides were incubated overnight at 4°C with the primary antibody (for CD3: clone SP7 abcam ab16669; for CD4: clone 4SM95 ThermoFisher Scientific #14-9766-82; for CD8: clone 4SM15 ThermoFisher Scientific #14-0808-82; for Foxp3: clone FJK-16s ThermoFisher Scientific #14-5773-82; for PD-1: clone EPR20665 abcam ab214421). The sections were incubated with the biotinylated secondary antibody (for CD3 and PD-1: Vector Laboratories BA-1100; for CD4, CD8, and Foxp3: Vector Laboratories BA-9401) for 30 minutes at room temperature. The Vectastain Elite ABC kit (Vector Laboratories) was used for the avidin-biotin complex formation. Slides were incubated with the avidin-biotin complex for 30 minutes at room temperature. The 3,3′-diaminobenzidine tetra hydrochloride chromogen (DAKO) reaction was allowed to develop for 5 seconds up to 15 minutes under visual microscopy control, depending on the antibody used. Hematoxylin was used to counterstain the sections, and the slides were covered with a cover glass-mounted with AquaTex.

RNA sequencing analysis. Total RNA for library preparation and sequencing analysis was purified from microdissected *VcMsh2* FFPE tumor and normal intestinal tissue using the FFPE RNA Isolation Kit (Qiagen) that included a genomic DNA elimination step. Coding RNA transcripts were enriched using mouse exome panel hybridization (Twist Biosciences). Size, concentration, and integrity was verified using Agilent 2100 Bioanalyzer (Agilent Technologies). Libraries were generated using Illumina's TruSeq RNA sample Prep Kit v3, following manufacturer's protocol. Sequencing of 8–10 pM of each library was done on the NovaSeq sequencer as 75-bp paired-end read runs.

Quality control of raw sequencing reads was performed with fastqc.[1] Spliced alignment of the reads to the reference genome was accomplished with STAR,[2] followed by a second round of quality control using RSeQC.[3] Mouse genome build Mm.10 and the corresponding GENCODE annotation, version 25, were used as reference. Mapped reads were quantified at the gene level as a raw count matrix using featureCounts from Subread[4] using fracOverlap 1 (only entire reads overlapping to annotation feature are counted). Raw feature counts were normalized and differential expression analysis carried out using DESeq2,[5] excluding genes mapping to mitochondria. Differential expression rank order was used for subsequent gene set enrichment analysis, performed using the clusterProfiler package in R. Gene sets queried included the Hallmark, Canonical Pathways, and GO Biological Processes Ontology collections available through the Molecular Signatures Database.[6]

Supplementary References

1. Wingett SW, Andrews S. FastQ Screen: a tool for multi-genome mapping and quality control. F1000Res 2018; 7:1338.
2. Dobin A, Davis CA, Schlesinger F, et al. STAR: ultrafast universal RNA-seq aligner. Bioinformatics 2013;29:15–21.
3. Wang L, Wang S, Li W. RSeQC: quality control of RNA-seq experiments. Bioinformatics 2012;28:2184–2185.
4. Liao Y, Smyth GK, Shi W. The Subread aligner: fast, accurate and scalable read mapping by seed-and-vote. Nucleic Acids Res 2013;41:e108.
5. Love MI, Huber W, Anders S. Moderated estimation of fold change and dispersion for RNA-seq data with DESeq2. Genome Biol 2014;15:550.
6. Subramanian A, Kuehn H, Gould J, et al. GSEA-P: a desktop application for Gene Set Enrichment Analysis. Bioinformatics 2007;23:3251–3253.
7. Chang K, Taggart MW, Reyes-Uribe L, et al. Immune profiling of premalignant lesions in patients with Lynch Syndrome. JAMA Oncol 2018;4:1085–1092.
8. Bommi PV, Bowen CM, Reyes-Uribe L, et al. The transcriptomic landscapes of mismatch repair-deficient intestinal stem cells. Cancer Res 2021;81:2760–2773.

Repeat	Mutation Frequency	FSP (-1) Freq	FSP (-2) Freq	Polymorphic
Ncad	75%	56.25%	37.50%	no
Xirp1	37.50%	31.25%	6.25%	no
5730596B20Rik	37.50%	37.50%	0.00%	no
Rif1	33.30%	20.00%	13.33%	no
Maz	33.30%	20.00%	13.33%	no
Hic1	31.25%	18.75%	12.50%	no
Sdccag1	25%	25.00%	6.25%	no
Tmem107	25%	25.00%	6.25%	no
Srcin1	25%	25.00%	0.00%	no
Marcks	20%	20.00%	0.00%	no
Senp6	18.75%	18.75%	0.00%	no
Phactr4	18.75%	18.75%	0.00%	no
Chrnb2	18.75%	12.50%	6.25%	no
Ccdc112	14.30%	n.a.	n.a.	no
Grb14	12.50%	n.a.	n.a.	no
Smap1	12.50%	n.a.	n.a.	no
Cdkl3	12.50%	n.a.	n.a.	no
A230052G05Rik	12.50%	n.a.	n.a.	no
Zfand4	12.50%	n.a.	n.a.	no
Fam71a	12.50%	n.a.	n.a.	no
Il1f9	12.50%	n.a.	n.a.	no
C79407	6.67%	n.a.	n.a.	no
Spice1	6.25%	n.a.	n.a.	no
Dclre1c	6.25%	n.a.	n.a.	no
Bud13	6.25%	n.a.	n.a.	no
Slc35f5	6.25%	n.a.	n.a.	no
Chd2	6.25%	n.a.	n.a.	no
Tgfb1i1	73.30%	n.a.	n.a.	yes
Defb34	31.25%	n.a.	n.a.	yes
Kcnma1	25%	n.a.	n.a.	yes
RIKC030005K15	25%	n.a.	n.a.	yes
Rfc3	18.75%	n.a.	n.a.	yes
Glrx2	18.75%	n.a.	n.a.	yes
Elavl3	12.50%	n.a.	n.a.	yes
Otu1	12.50%	n.a.	n.a.	yes
Armcx5	6.30%	n.a.	n.a.	yes
Glis2	0.00%	n.a.	n.a.	no
Ddhd2	0.00%	n.a.	n.a.	no
Cd300c	0.00%	n.a.	n.a.	no
Adamtsl1	0.00%	n.a.	n.a.	no
Rgs12	0.00%	n.a.	n.a.	no
Grk4	0.00%	n.a.	n.a.	no
Fam60a	0.00%	n.a.	n.a.	no
Zfp457	0.00%	n.a.	n.a.	no
Aim2	0.00%	n.a.	n.a.	no
Esp31	0.00%	n.a.	n.a.	yes
Ptpn21	0.00%	n.a.	n.a.	yes
Smarcc2	0.00%	n.a.	n.a.	yes
Cyp4a30b	0.00%	n.a.	n.a.	yes
Wfdc8	0.00%	n.a.	n.a.	yes
B2m-1-Sequ	0.00%	n.a.	n.a.	yes
Lrp5	0.00%	n.a.	n.a.	yes
Mndal	0.00%	n.a.	n.a.	yes
Ist1	0.00%	n.a.	n.a.	yes
Bcas3	0.00%	n.a.	n.a.	yes
Eml2	0.00%	n.a.	n.a.	yes

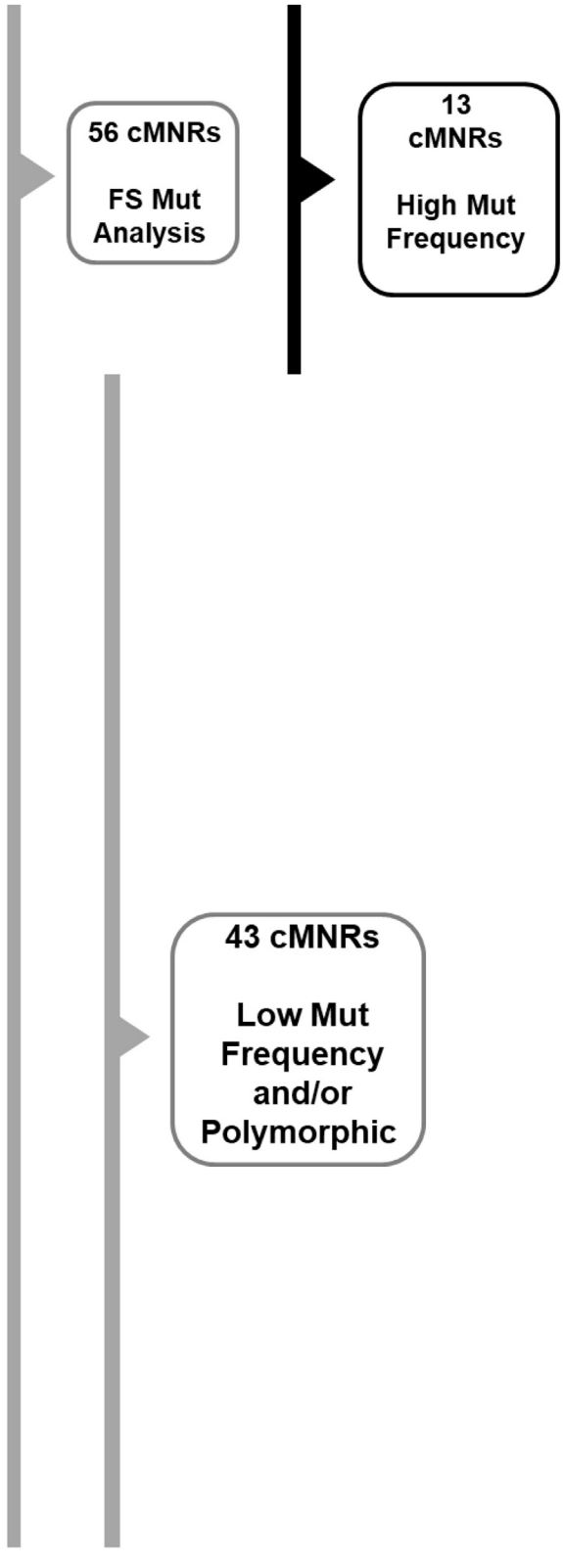

Supplementary Figure 1. Mutation frequency of coding microsatellites derived from mouse genome analysis.

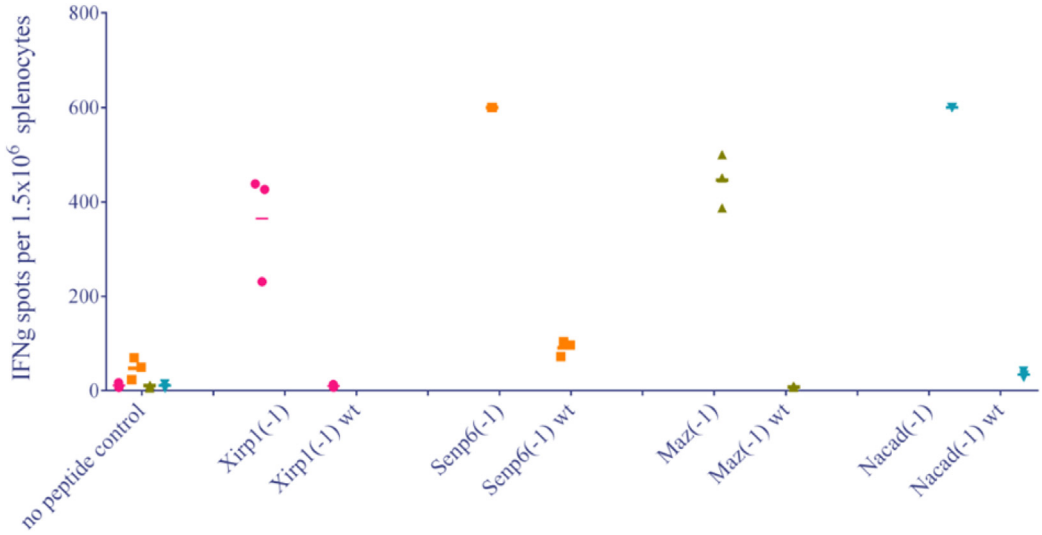

Supplementary Figure 2. Cross-reactivity with wild-type peptides. IFN-gamma (IFN-g) ELISpot was carried out with the wild-type peptide and the corresponding FSP of interest using splenocytes from immunized mice. The mean number of cells that are secreting IFN-g per 1.5×10^6 cells per mouse is shown on the y-axis and the FSPs and wild-type peptides are indicated on the x-axis.

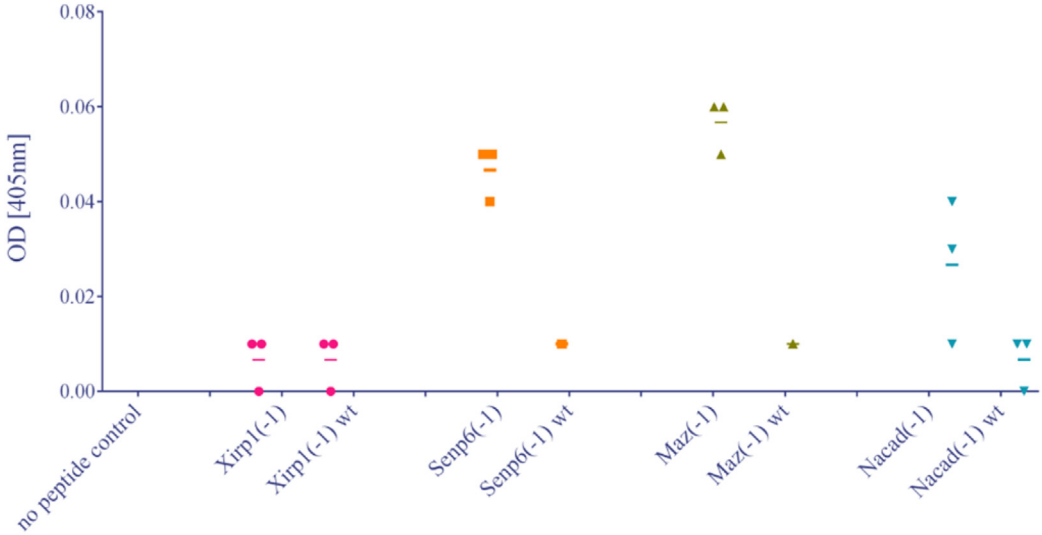

Supplementary Figure 3. Humoral immune responses. Serum (50 μL) from vaccinated mice was analyzed by peptide-specific (FSPs and wild-type peptides) total IgG ELISA. Optical density (OD) was measured at 405 nm in an ELISA reader with a reference wavelength of 620 nm. The mean OD value is shown for each mouse.

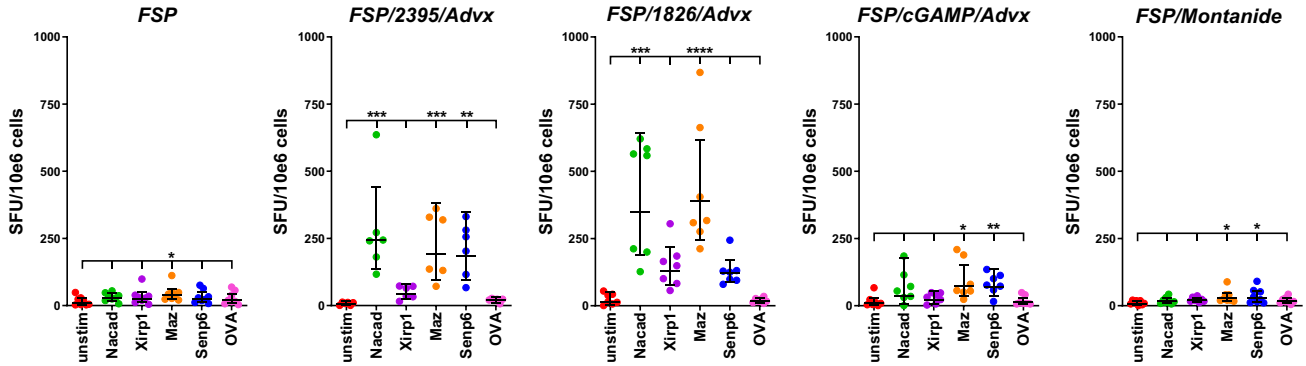

Supplementary Figure 4. Adjuvant promotion of FSP-specific T cell responses. Mice were immunized subcutaneously in inguinal area with 200 μg FSP peptide pool alone or adjuvanted with 20 μg CpG-2395 + 50% v/v AddaVax, 20 μg CpG-1826 + 50% v/v AddaVax, 15 μg 2'3'-cGAMP + 50% v/v AddaVax, or 70% v/v Montanide on days 0, 14, and 28. Spleens were harvested on day 42 and splenocytes restimulated in vitro with individual FSP peptides or OVA peptide as a negative control for 48 hours and spot-forming units (SFUs)/1^{e6} cells analyzed via ELISpot. Data are reported as geometric means + 95% confidence intervals. Statistical comparisons are between unstimulated cells and all other groups and were generated using 1-way analysis of variance nonparametric analysis with the Kruskal-Wallis multiple comparisons test. *$P < .05$; **$P < .01$; ***$P < .001$; ****$P < .0001$.

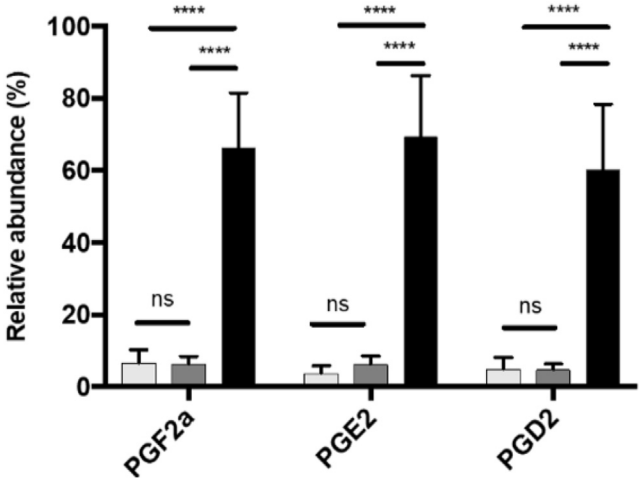

Supplementary Figure 5. Prostaglandin expression. Relative abundance of inflammatory prostaglandins in intestinal mucosae of mice vaccinated with FSP alone (*black bar*) or in combination with ASA (*light gray bar*) or NAP (*dark gray bar*). SD and significance levels are indicated (****$P < .00001$). ns, not significant.

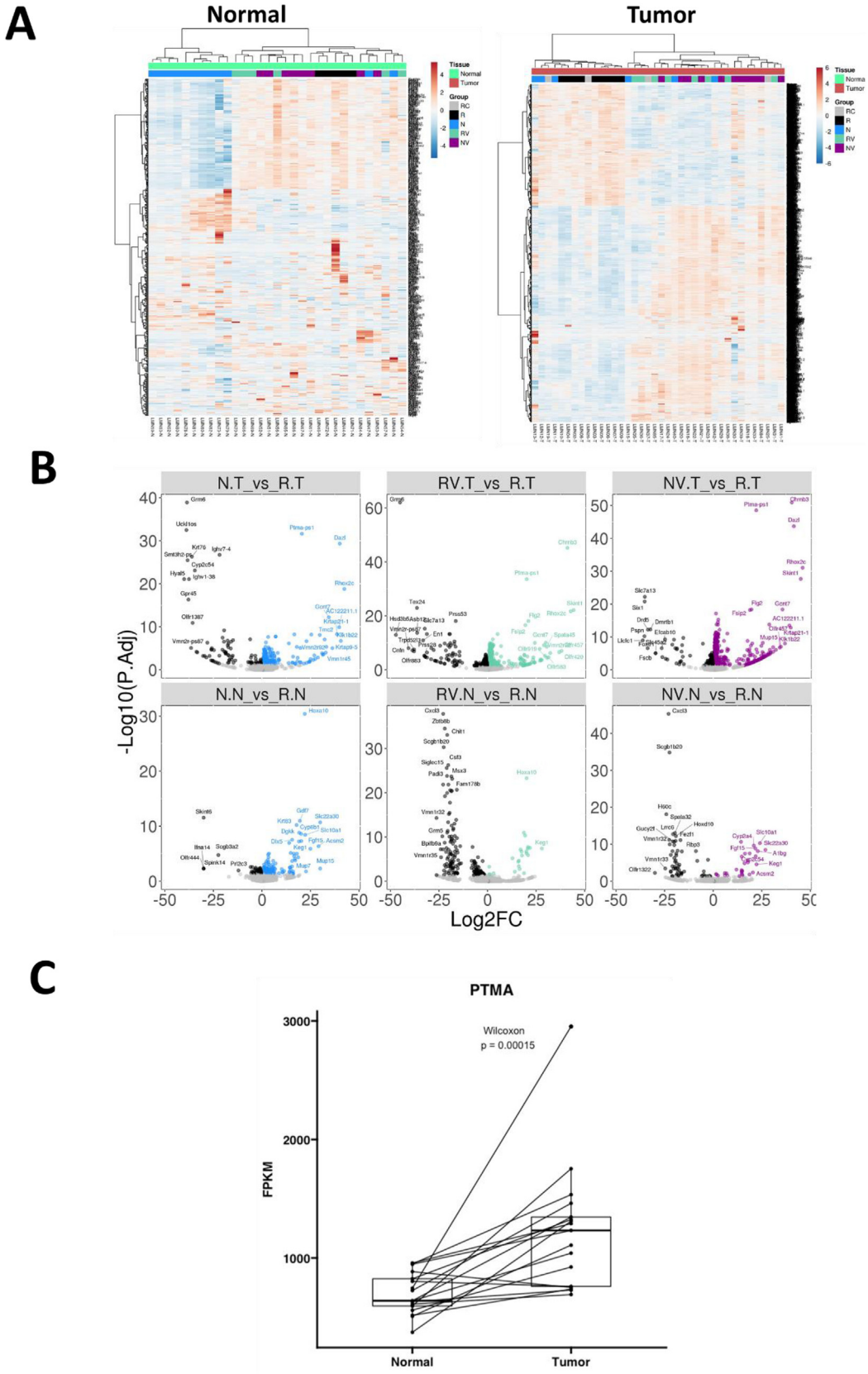
A
Normal
Tumor
Tissue
Normal
Tumor
Group
RC
R
N
RV
NV
B
N.T_vs_R.T
RV.T_vs_R.T
NV.T_vs_R.T
N.N_vs_R.N
RV.N_vs_R.N
NV.N_vs_R.N
-Log10(P.Adj)
Log2FC
C
PTMA
Wilcoxon
p = 0.00015
FPKM
Normal
Tumor

Supplementary Figure 6. Transcriptional profiling of tumors (T) and normal intestinal tissue (N) derived from untreated *VcMsh2* mice on Western diet (R), treated with NAP or ASA (NSAID; N), treated with FSP vaccine (RV), or combination NSAID and FSP vaccine (NV). (*A*) *Heatmap* representing all identified differentially expressed genes (false discovery rate [FDR]–adjusted *P* value $< .05$) between treatment groups and untreated mice in normal tissue (*left*) and tumor tissue (*right*). (*B*) *Volcano plots* depicting differential expression patterns identified in treated mice relative to untreated mice in tumor tissue (*top*) and normal tissue (*bottom*). Genes with significantly changing expression (FDR-adjusted *P* value $< .05$) with treatment are shown in *color* as labeled in (*A*). (*C*) RNA transcript levels for PTMA in human LS patient normal colorectal mucosa and colorectal adenomas/adenocarcinomas, measured in re-analysis of RNA sequencing data published in Chang et al[7] and Bommi et al.[8]

A. GSEA Enrichment R.T vs R.N

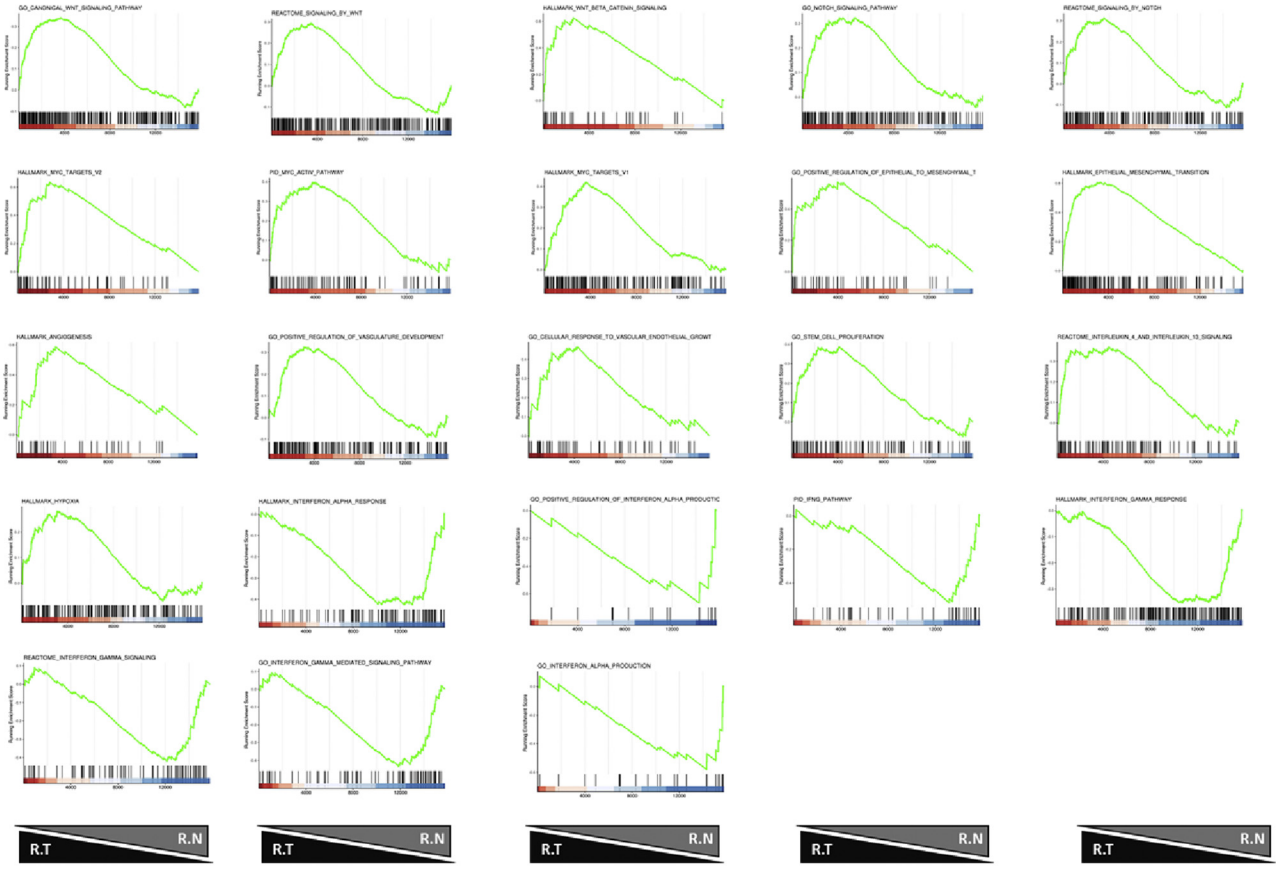

	NES	pvalue	p.adjust
HALLMARK_ANGIOGENESIS	2.23	2.62E-04	1.12E-02
HALLMARK_WNT_BETA_CATENIN_SIGNALING	2.45	2.66E-04	1.12E-02
GO_POSITIVE_REGULATION_OF_EPITHELIAL_TO_MESENCHYMAL_TRANSITION	2.30	2.73E-04	1.12E-02
GO_CELLULAR_RESPONSE_TO_VASCULAR_ENDOTHELIAL_GROWTH_FACTOR_STIMULUS	1.96	2.79E-04	1.12E-02
HALLMARK_MYC_TARGETS_V2	2.69	2.82E-04	1.12E-02
HALLMARK_INTERFERON_ALPHA_RESPONSE	-1.81	2.93E-04	1.12E-02
GO_STEM_CELL_PROLIFERATION	1.85	3.29E-04	1.12E-02
GO_NOTCH_SIGNALING_PATHWAY	1.67	3.72E-04	1.12E-02
GO_POSITIVE_REGULATION_OF_VASCULATURE_DEVELOPMENT	1.69	3.73E-04	1.12E-02
HALLMARK_EPITHELIAL_MESENCHYMAL_TRANSITION	3.17	3.88E-04	1.12E-02
HALLMARK_MYC_TARGETS_V1	2.19	3.94E-04	1.12E-02
HALLMARK_INTERFERON_GAMMA_RESPONSE	-1.66	4.02E-04	1.12E-02
GO_CANONICAL_WNT_SIGNALING_PATHWAY	1.88	4.85E-04	1.12E-02
PID_MYC_ACTIV_PATHWAY	1.79	6.00E-04	1.17E-02
GO_INTERFERON_GAMMA_MEDIATED_SIGNALING_PATHWAY	-1.77	6.01E-04	1.17E-02
PID_IFNG_PATHWAY	-1.87	6.41E-04	1.20E-02
GO_POSITIVE_REGULATION_OF_INTERFERON_ALPHA_PRODUCTION	-1.95	6.86E-04	1.22E-02
REACTOME_SIGNALING_BY_NOTCH	1.62	7.41E-04	1.24E-02
REACTOME_SIGNALING_BY_WNT	1.59	8.96E-04	1.32E-02
REACTOME_INTERLEUKIN_4_AND_INTERLEUKIN_13_SIGNALING	1.74	9.47E-04	1.35E-02
REACTOME_INTERFERON_GAMMA_SIGNALING	-1.71	1.65E-03	1.95E-02
GO_INTERFERON_ALPHA_PRODUCTION	-1.81	2.86E-03	2.85E-02
HALLMARK_HYPOXIA	1.46	3.49E-03	3.28E-02

Supplementary Figure 7. Gene set enrichment analysis (GSEA) enrichment plots and scores. (*A*) Selected GSEA enriched pathways comparing control mouse intestinal tumors and normal tissue (R.T vs. R.N). (*B*) Selected GSEA enriched pathways comparing NSAID-treated mouse intestinal tumors and normal tissue (N.T vs. N.N). (*C*) Selected GSEA enriched pathways comparing FSP vaccinated mouse intestinal tumors and normal tissue (RV.T vs RV.N).

B. GSEA Enrichment N.T vs N.N

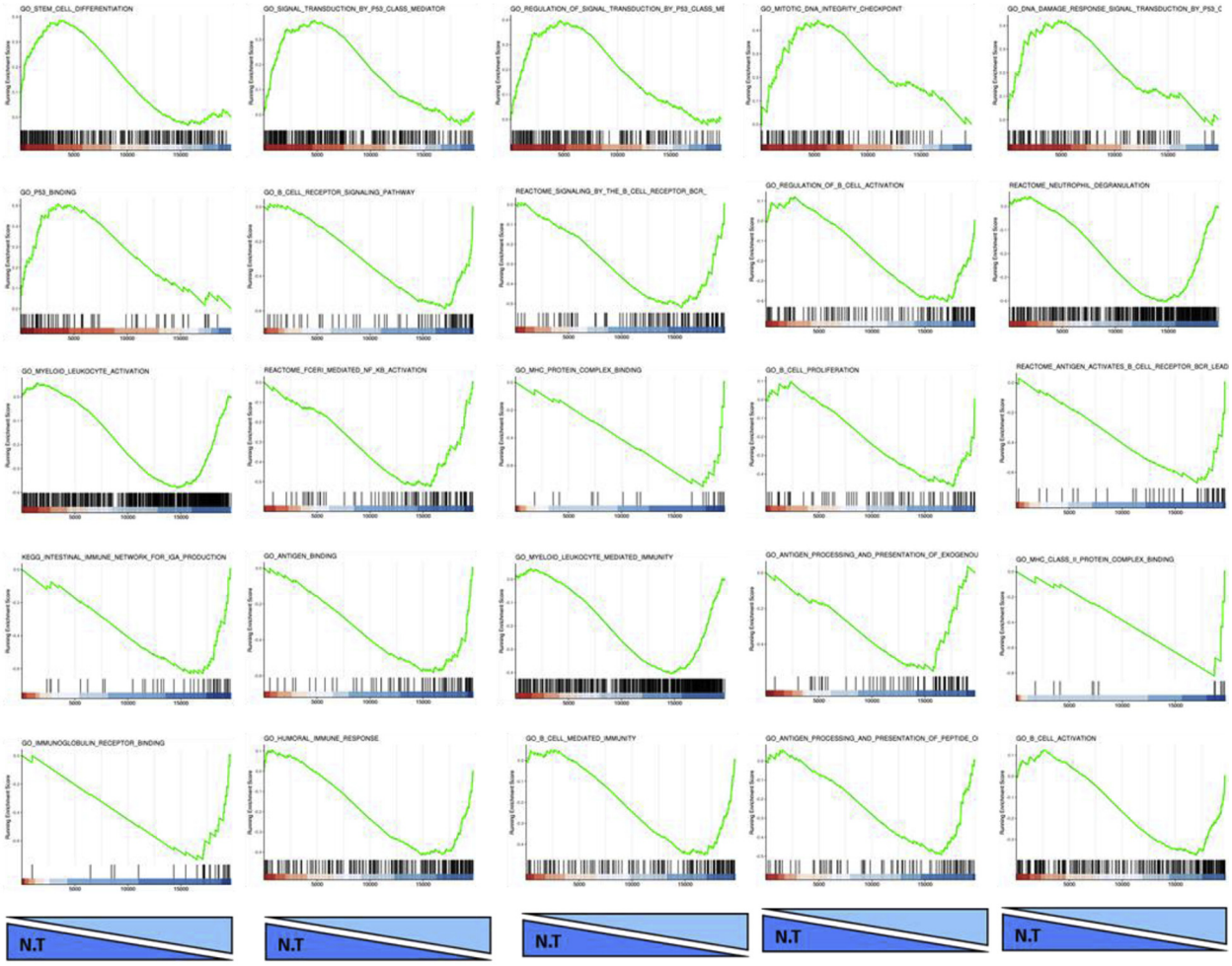

	NES	pvalue	p.adjust
GO_MYELOID_LEUKOCYTE_ACTIVATION	-1.79	1.23E-04	4.46E-03
GO_MYELOID_LEUKOCYTE_MEDIATED_IMMUNITY	-1.88	1.26E-04	4.46E-03
REACTOME_NEUTROPHIL_DEGRANULATION	-1.86	1.28E-04	4.46E-03
GO_B_CELL_ACTIVATION	-1.63	1.38E-04	4.46E-03
GO_HUMORAL_IMMUNE_RESPONSE	-1.79	1.39E-04	4.46E-03
GO_B_CELL_MEDIATED_IMMUNITY	-1.84	1.49E-04	4.46E-03
REACTOME_SIGNALING_BY_THE_B_CELL_RECEPTOR_BCR_	-2.09	1.50E-04	4.46E-03
REACTOME_FCERI_MEDIATED_NF_KB_ACTIVATION	-2.02	1.54E-04	4.46E-03
GO_ANTIGEN_PROCESSING_AND_PRESENTATION_OF_PEPTIDE_OR_POLYSACCHARIDE_ANTIGEN_VIA_MHC_CLASS_II	-1.89	1.55E-04	4.46E-03
GO_ANTIGEN_PROCESSING_AND_PRESENTATION_OF_EXOGENOUS_PEPTIDE_ANTIGEN_VIA_MHC_CLASS_I	-2.04	1.58E-04	4.46E-03
GO_ANTIGEN_BINDING	-2.14	1.58E-04	4.46E-03
GO_B_CELL_RECEPTOR_SIGNALING_PATHWAY	-2.18	1.58E-04	4.46E-03
KEGG_INTESTINAL_IMMUNE_NETWORK_FOR_IGA_PRODUCTION	-2.08	1.64E-04	4.46E-03
REACTOME_ANTIGEN_ACTIVATES_B_CELL_RECEPTOR_BCR_LEADING_TO_GENERATION_OF_SECOND_MESSENGERS	-2.25	1.64E-04	4.46E-03
GO_IMMUNOGLOBULIN_RECEPTOR_BINDING	-2.15	1.69E-04	4.46E-03
GO_MHC_PROTEIN_COMPLEX_BINDING	-2.19	1.70E-04	4.46E-03
GO_MHC_CLASS_II_PROTEIN_COMPLEX_BINDING	-2.14	1.76E-04	4.46E-03
GO_DNA_DAMAGE_RESPONSE_SIGNAL_TRANSDUCTION_BY_P53_CLASS_MEDIATOR	1.78	2.91E-04	4.46E-03
GO_MITOTIC_DNA_INTEGRITY_CHECKPOINT	1.87	2.92E-04	4.46E-03
GO_REGULATION_OF_SIGNAL_TRANSDUCTION_BY_P53_CLASS_MEDIATOR	1.81	3.31E-04	4.46E-03
GO_SIGNAL_TRANSDUCTION_BY_P53_CLASS_MEDIATOR	1.80	3.74E-04	4.46E-03
GO_STEM_CELL_DIFFERENTIATION	1.84	3.75E-04	4.46E-03
GO_P53_BINDING	1.98	5.36E-04	5.01E-03
GO_B_CELL_PROLIFERATION	-1.76	6.27E-04	5.46E-03
GO_REGULATION_OF_B_CELL_ACTIVATION	-1.64	8.95E-04	7.11E-03

Supplementary Figure 7. Continued

C. GSEA Enrichment Plots: RV.T vs RV.N (Upregulated)

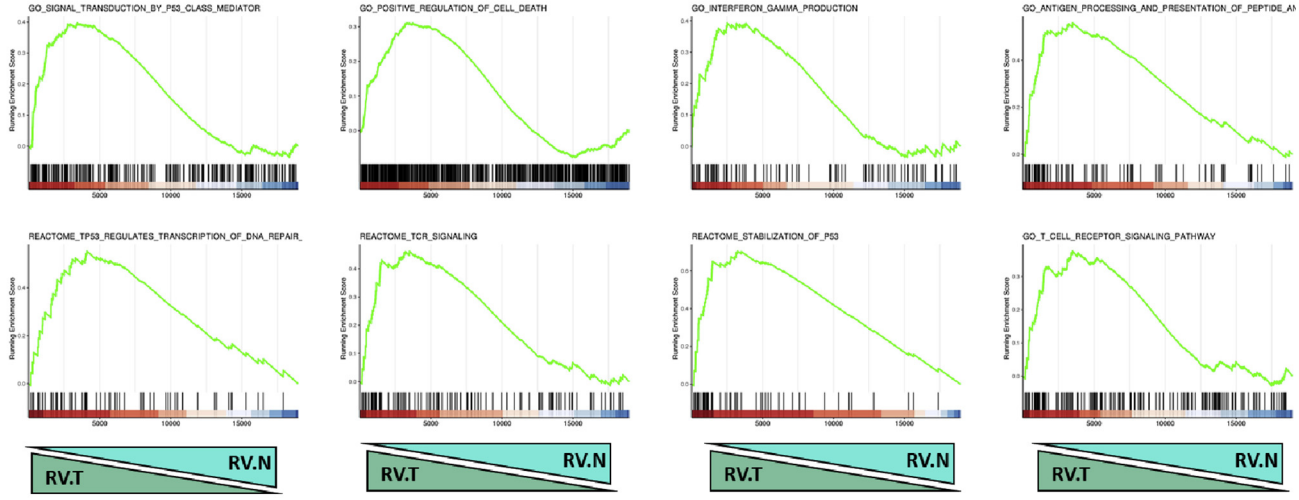

	NES	pvalue	p.adjust
GO_SIGNAL_TRANSDUCTION_BY_P53_CLASS_MEDIATOR	1.75	1.25E-04	3.80E-03
REACTOME_TCR_SIGNALING	1.83	1.41E-04	3.80E-03
GO_ANTIGEN_PROCESSING_AND_PRESENTATION_OF_PEPTIDE_ANTIGEN_VIA_MHC_CLASS_I	2.14	1.45E-04	3.80E-03
REACTOME_STABILIZATION_OF_P53	2.48	1.55E-04	3.80E-03
GO_POSITIVE_REGULATION_OF_CELL_DEATH	1.47	2.19E-04	4.71E-03
REACTOME_TP53_REGULATES_TRANSCRIPTION_OF_DNA_REPAIR_GENES	1.98	3.05E-04	5.89E-03
GO_T_CELL_RECEPTOR_SIGNALING_PATHWAY	1.60	1.17E-03	1.55E-02
GO_INTERFERON_GAMMA_PRODUCTION	1.52	9.35E-03	6.98E-02

Supplementary Figure 7. Continued

Supplementary Table 1. List of cMNR Primers

Gene	Primer (5′ > 3′) Antisense; Sense
Adamtsl1_A1	CTG GAT GTC CTC CTC CAC AC
Adamtsl1_S1	CTG ATG ACG CCC CTT GCT TC
Armcx5_A1	CCA GTT CCC ATC TGG AGG TA
Armcx5_S1	TGA ACC CCC AGA TAC ATT CG
Bcas3_A1	ACG CAG GCT TTG TTA CTG TT
Bcas3_S1	TCC GTG TAC TTC TGG AGC AT
C79407A	ATA CGT GAT GCT GGC CTT TT
C79407S	AAG ACC AGA CAG GAA ACA GCA
Ccdc112_A1	GCA CAC TGA CAC GCA CAA T
Ccdc112_S1	CGG GAA GAA CTC TGG ATG AA
Cd300c_A1	CTG AGG CAC TGG TCT TGA CA
Cd300c_S1	ACT GTG GGG GAG TCA CTC AG
Chd2_A1	ATG CAG GGA CGG TAA AGA CA
Chd2_S1	CAA GAT CTC TGG GGT TCA GG
Chrnb2_A1	TGC CAG TTC CCA CAT AGG AT
Chrnb2_S1	TGC TGC CAG ACA ATC ACA TT
Cyp4a30b_A1	CCC TGA GCG GTT AAA CTG AG
Cyp4a30b_S1	CAT CAA GTC CCT CCA GCA GT
Eml2_A1	GTC GTA GAG GCC GCA GAA
Eml2_S1	GAA CGA AGG GCG TTG CTA T
Esp31_A1	CAC TGG GTC CAT TAC TTG GAG
Esp31_S1	TCC TGA GAT GTC ATT CAA CCT C
Fam60a_A1	TCC TAA ATT GGG GAT GGT GA
Fam60a_S1	TGC TGC TTG TGA AAA GAT GG
Fam71a_A1	GCT TTT GAC GCT GAC CTT GT
Fam71a_S1	AGT ACC TAT GCC ATC CCA GC
Grb14_A	GGC TGA GGC TTG CTT TAC TC
Grb14_S	GCA TTT GCA GCT TTT CAG TG
Grk4_A1	CAT GGC TTC ACC TTT CCT CT
Grk4_S1	AAA CTA GGT TTG TGC CTG TCA AG
Il1f9_A1	AGC CAT ACC TGA GAT GTG TGT
Il1f9_S1	GGC ACC AGA ACA AGA TCA CG
Kcnma1_A	TGC TTA CCT CAT CAG CTT CG
Kcnma1_S	CAC AAG CTG CCT GTA TTT GC
m5730596B20Rik_A1	TCA ATG AGG AGA ATG TGC AGA C
m5730596B20Rik_S1	CAG GTT GGA CTC ACT GGG TC
mA230052G05Rik_A1	GTC TCA GAC CGT GGC AGA AG
mA230052G05Rik_S1	GCT CTG TCC TGC TTT GTC CT
Maz_A1	CAA AGA AGC GGG ACT GGA G
Maz_S1	GTT CCC CGT GTT CCC TTG
mB2m_A1	TCCTTGCTGAAGGACATATCTGA
mB2m_S1	GAGAATGGGAAGCCGAACAT
mBud13_A1	CTT GGT CTG TTC CGT GGT G
mBud13_S1	CAC AGG AGA TTT CAT AGA CGC TT
mCdkl3_A1	AGG AAG GAA TTG TCA AGC TTG T
mCdkl3_S1	GGC GAT TGT GAG GGG AAG AA
mDclre1c_A1	CAC CTG CCT TGC CTC TAC C
mDclre1c_S1	CAT TCA CAT GCG CAC ACA CA
mDdhd2_A1	TCT AAA TCT TCG CCT TAC CTT TGG
mDdhd2_S1	GGA TAC GTA CAT GCT TGC AGT
mDefb34_A1	TCT CCC ATT AAT CCT GCT GCA
mDefb34_S1	AGC CAC ATG TGA AGC AGA GT
mElavl3_A1	GTC AGT GGC TCC ATT TGT CC
mElavl3_S1	CGG GTA CGA CCT GTT TTC TC
mGlis2_A1	GGT GAG AGG CAC TTG TCC TT
mGlis2_S1	TTC CAG CCA CTT CGC TAT TT
mGlrx2_A1	TGG CGA CTA TCC ACA TCA TTC A
mGlrx2_S1	GGA CAC TCA CAG GCT TCA CA
mHic1_A1	AGA TAT CGG ACC TGG GAG TCC
mHic1_S1	TCC CTG GCT TAA GAG TTC CTC
mLrp5_A1	GGG AAG AGG TGG CAG TAA CTC
mLrp5_S1	CCT GGA CTT GAA TTC GGA CT
mMarcks_A1	GGT CGC TCC CTC TGC TTC AG
mMarcks_S1	GTC CGC CTC CTC CAC GTC
Mndal_A1	CCT GAT CCT GGG TGA GCT TA
Mndal_S1	TCA GGG TTC AAT TTC CAA CAC A
mRif1_A1	ACA TAC TTT GGC CGA CAG TTT C
mRif1_S1	GGC ATG GAA AGA AAA TCA AGT GG
mSlc35f5_A1	CCC CAC ACA GCA CAC ACA T
mSlc35f5_S1	AGA CTG TAG GGA AAT TGA CTG C
mSmap1_A1	GGC TTT TCT GGC TCC TTT TCT C
mSmap1_S1	AGT CTG TTC TGT TGG ACA TGT GA
mSpice1_A1	TGT GGG CAG AGA GAG CAA AC
mSpice1_S1	TCT GAG TCT CTA GTG GGC TCA
mSrcin1_A1	AAA ATC CAA GCC TTT GCT GA
mSrcin1_S1	CTG CTC CTC ACT CTC CCA AC
mTmem107_A1	TCT AGG TGG GGG AAA CCT TC
mTmem107_S1	GAG CGA TGG GAA TGT ACC AC

Supplementary Table 1. Continued

Gene	Primer (5′ > 3′) Antisense; Sense
mXirp1_A1	GCC AAC TCG CTC ATA GGG TA
mXirp1_S1	CCA CCA ACA AGA GCA ACA GA
Nacad_A1	CTG TCC CTC TGT CCG TCA AT
Nacad_S1	ACG CTC ACT CGG CTT GAT AG
Phactr4_A	CCA GGG CTT TGC TCA AAC TA
Phactr4_S	ATC TTC AAG CCG TGG AAA TG
Ptpn21_A	CGC TCT GGT GGA CAC TTC TT
Ptpn21_S	TTT GAA AGG TGT CTG GGT ACG
Rfc3_A	AGG AGC AGT TTA CCT GGG ATT
Rfc3_S	TTG GCA GTA GTG ATT TGG TGA
Rgs12_A1	GGC AGA GCA GGT TTA AGG ACT
Rgs12_S1	CCG CCT TTC AAA GAG AGA AG
RIKC030005K15_A1	AGC TTA GGG AGG AAG GCT GT
RIKC030005K15_S1	GAG ACA GTG TTT CAA AAA TCT CCA
Sdccag1_A	CTG ACA GGC TGA GAT CCA CA
Sdccag1_S	GCC AGC ATT GAG AAC AGT GA
Senp6_A	CAA ATG TCC TGG CAC GTA GA
Senp6_S	GTG AGC CTT GTT ACC GGA GA
Smarcc2_A1	TCC CTT CAA AGG AAC CAG AA
Smarcc2_S1	CAG CCA CAA CAA GCT GGA G
Tgfb1i1_A1	GCC GTG ACC ATG TAT GGA A
Tgfb1i1_S1	ACA GAG CCA CAA AGC TGG AT
Wfdc8_A1	GTG TTA GCG GTG CTG AGG A
Wfdc8_S1	TCT CGC CTC ACA GAC AAC TG
Zfand4_A1	GTG GGT GGG TAG GGA ATT G
Zfand4_S1	CCT AAA GTG CCA GAG GGA TG
Zfp457_A1	TGG GTA TGG GGG ACT TTT G
Zfp457_S1	TGT GGC AAG GAC TTC CAT TA